

Buzz Killington



AIAA Design/Build/Fly
2013-2014
Design Report

 Georgia Institute
of Technology®



TABLE OF CONTENTS

1. EXECUTIVE SUMMARY	4
1.1 DESIGN PROCESS	4
1.2 KEY MISSION REQUIREMENTS AND DESIGN FEATURES	4
1.3 PERFORMANCE CAPABILITIES OF THE SYSTEM	5
2. MANAGEMENT SUMMARY	6
2.1 TEAM ORGANIZATION	6
2.2 MILESTONE CHART	6
3. CONCEPTUAL DESIGN.....	7
3.1 MISSION REQUIREMENTS	7
3.2 TRANSLATION INTO DESIGN REQUIREMENTS	14
3.3 CONFIGURATIONS CONSIDERED	15
3.4 COMPONENT WEIGHTING/SELECTION PROCESS.....	16
3.5 FINAL CONCEPTUAL DESIGN CONFIGURATION	19
4. PRELIMINARY DESIGN	20
4.1 DESIGN METHODOLOGY	20
4.2 DESIGN TRADES.....	20
4.3 MISSION MODEL.....	22
4.4 AERODYNAMIC CHARACTERISTICS	23
4.5 STABILITY AND CONTROL.....	27
4.6 MISSION PERFORMANCE	29
5. DETAIL DESIGN	29
5.1 FINAL DESIGN	29
5.2 STRUCTURAL CHARACTERISTICS	30
5.3 SYSTEM AND SUBSYSTEM DESIGN/COMPONENT/SELECTION/INTEGRATION	32
5.4 WEIGHT AND BALANCE	36
5.5 FLIGHT AND MISSION PERFORMANCE	37
5.6 DRAWING PACKAGE	40
6. MANUFACTURING PLAN AND PROCESSES.....	45
6.1 MANUFACTURING PROCESSES INVESTIGATED	45
6.2 MANUFACTURING PROCESSES SELECTED	46
6.3 MANUFACTURING MILESTONES.....	48
7. TESTING PLAN	48
7.1 OBJECTIVES AND SCHEDULES.....	49
7.2 PROPULSION TESTING.....	49
7.3 PAYLOAD LOADING AND RELEASE TESTING.....	50
7.4 STRUCTURAL TESTING.....	51
7.5 FLIGHT TESTING.....	51
7.6 CHECKLISTS.....	52
8. PERFORMANCE RESULTS	53
8.1 COMPONENT AND SUBSYSTEM PERFORMANCE	53
8.2 SYSTEM PERFORMANCE	56
9. REFERENCES	59



ACRONYMS AND NOMENCLATURE

C.G.	– Center of Gravity	e	– Oswald Efficiency
RAC	– Rated Aircraft Cost	P	– Power
TFS	– Total Flight Score	S	– Area
GS	– Ground Score	K_V	– Motor Voltage Constant (V)
EW	– Empty Weight	K_D	– Wing Loading Dissipative Constant
TMS	– Total Mission Score	K_T	– Thrust Loading Dissipative Constant
M1	– Mission One	K_A	– Regressive Constant
M2	– Mission Two	\dot{x}	– Position Derivative with respect to time
M3	– Mission Three	V	– Velocity
FOM	– Figures of Merit	\dot{V}	– Velocity Derivative with respect to time
FS	– Flight Score	m	– mass
TOFL	– Takeoff Field Length	T	– Thrust
S_g	– Takeoff Roll Distance	D	– Drag
NiCad	– Nickel-Cadmium	\bar{p}	– Dimensionless Rolling Rate
NiMH	– Nickel-Metal Hydride	\bar{q}	– Dimensionless Pitching Rate
AVL	– Athena Vortex-Lattice	\bar{r}	– Dimensionless Yawing Rate
\tilde{C}_L	– Airfoil Section Lift Coefficient	AR	– Aspect Ratio
\tilde{C}_D	– Airfoil Section Drag Coefficient	R_e	– Reynolds Number
\tilde{C}_m	– Airfoil Section Moment Coefficient	R_T	– Taper Ratio
C_L	– Aircraft Lift Coefficient	S_w	– Wing Area (ft ²)
C_D	– Aircraft Drag Coefficient	T_s	– Settling Time (s)
C_f	– Skin Friction Coefficient	ρ	– Density
C_Y	– Aircraft Side Force Coefficient	T_d	– Doubling Time (s)
C_n	– Aircraft Yawing Moment Coefficient	W	– Weight, lbs
C_m	– Aircraft Pitching Moment Coefficient	α	– Angle of Attack (degrees)
C_I	– Aircraft Rolling Moment Coefficient	β	– Sideslip Angle (degrees)
$C_{D,i}$	– Aircraft Induced Drag Coefficient	μ_r	– Rolling Coefficient of Friction
$C_{D,0}$	– Aircraft Zero-Lift Drag Coefficient	R_{ls}	– Wing Sweep
L'	– Wing Thickness Location Parameter	R_{wf}	– Wing Fuselage Interference



1. EXECUTIVE SUMMARY

This report details the design, testing, and manufacturing of the Georgia Institute of Technology *Buzz Killington* entry in the 2014-2015 AIAA Design/Build/Fly (DBF) competition. This aircraft was designed to successfully complete four tasks: a speed loading mission and three flight missions. The first flight mission consists of a high speed ferry flight with no payload. The second mission models the delivery of a sensor package and tests the maximum load capabilities of the aircraft by carrying a five pound payload internally through three laps. The third mission is a drop mission where a number of balls have to be carried externally and dropped one by one every lap.

1.1 Design Process

The primary objective for *Buzz Killington* is victory. This is achieved through the development of a light, fast aircraft that maximizes the flight score. Conceptual design of a winning aircraft began by translating the key mission requirements and scoring criteria into design requirements. These design requirements were used to determine an aircraft configuration that maximized the total flight score. The configuration was further defined in the preliminary design phase by comparing different motors, batteries, and propellers to achieve the required propulsion for the designed aircraft. Weight, drag, and aerodynamic coefficients were calculated and introduced into a flight simulation environment that estimated mission performance. The team used this data to conduct trade studies of wing loading, the propulsion system, payload capability, and takeoff distance to estimate the aircraft's maximum flight score. *Buzz Killington* then completed a detailed design by finalizing all dimensions, propulsion system components, and methods for component integration.

1.2 Key Mission Requirements and Design Features

A successful system design and score arise from the successful balance of key mission requirements. Specific design requirements were developed for each mission requirement and scoring element to maximize system performance and the overall competition score.

Empty Weight: The aircraft's empty weight is a significant driver of total score. Empty weight is comprised of the weight of the airframe and propulsion system. The entire aircraft was designed to be as minimalistic as possible without compromising the ability to complete all three flight missions. This was accomplished by determining the most efficient combination of airframe structure and propulsion system.

Number of Servos: The final flight score is inversely proportional to the number of servos on the aircraft. This competition defines a servo as any mechanical or electronic device used to control the airplane or payload release mechanism. Achieving the maximum flight score requires using the minimum number of servos required to control the aircraft. Various control surface configurations and drop mechanisms were analyzed to achieve the minimum number of servos.



Payload Requirement: Two of the three missions require the aircraft to carry a payload. Mission 2 (M2) requires a payload of five pounds to be carried internally. The access hatch for the internal payload must be easily accessible as this has a direct influence on the ground mission score. Mission 3 (M3) requires a number of balls to be carried externally. The number of balls carried in M3 has a large influence on the mission score, and define the number of laps required for the mission. The aircraft is designed to carry eight balls for M3.

Flight Time: Mission 1 (M1) requires that the aircraft complete as many laps along the designated flight path as possible within four minutes to maximize score, while M3 requires the aircraft to complete as many laps as the number of balls carried. For this reason, the propulsion system was designed to complete as many laps as balls carried while sustaining near full-throttle flight for the entire duration of the four minutes and minimizing propulsion system weight.

1.3 Performance Capabilities of the System

All of the specific design features created to maximize the performance of the system can be summarized by the following performance capabilities:

- Empty weight of 3 lbs.
- Reliable takeoff within 50 feet
- Four minute high-speed endurance
- Eight lap capability for M1
- 120 second flight time for M2
- Eight ball external capacity for M3
- Payload assembly in under 28 seconds
- Secure storage of required payloads
- Proven capability through two prototypes and seventeen test flights as shown in Figure 1.1
- Estimated RAC of 9.21 and a final score of 1.06

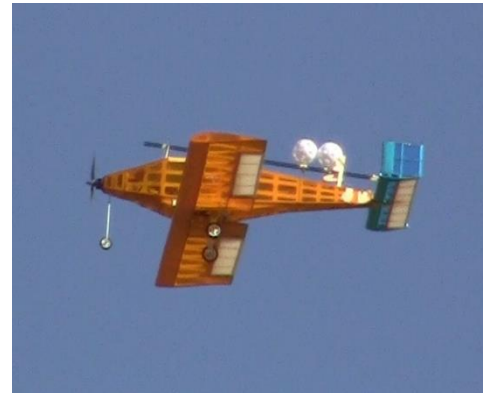


Figure 1.1: Aircraft in flight.

The final design was a conventional aircraft configuration with a low-wing placement, single motor, and tricycle gear. The aircraft was designed to simultaneously minimize weight, size, payload loading/unloading time, and takeoff distance, while maximizing speed and payload capabilities. The propulsion system was designed to provide enough power to fulfill ambitious performance characteristics, but weigh as little as possible. The aircraft's architecture and testing built on the teams' previous experience while continuing to push the envelope of practical, minimalistic design processes. *Buzz Killington* is confident that this design solution has been optimized to best accommodate all performance requirements and maximize total score.



2. MANAGEMENT SUMMARY

The *Buzz Killington* team consisted of twenty-six students: one graduate student, eight seniors, six juniors, three sophomores, and eight freshmen. Seventeen of the twenty-six students were returning members from the 2013-2014 Georgia Tech DBF entry. This team combines the right amount of manpower with the continued advantage of having a core of experienced members returning to build the team's knowledgebase and pass it on to newer members.

2.1 Team Organization

Buzz Killington used a hierachal structure to establish leadership and responsibility amongst its senior members, where responsibilities flow down to the team's newer members. This hierarchy served as an outline only, as all team members collaborated extensively to reach deadlines, share ideas, learn various disciplines, and produce a more successful aircraft. The work was divided during the design phase into CAD and Structures, Aerodynamics, Electrical and Propulsion, Payload, and Manufacturing. During construction, testing, and report writing, all team members participated fully. Figure 2.1 shows the different positions and the roles of each member of the team.

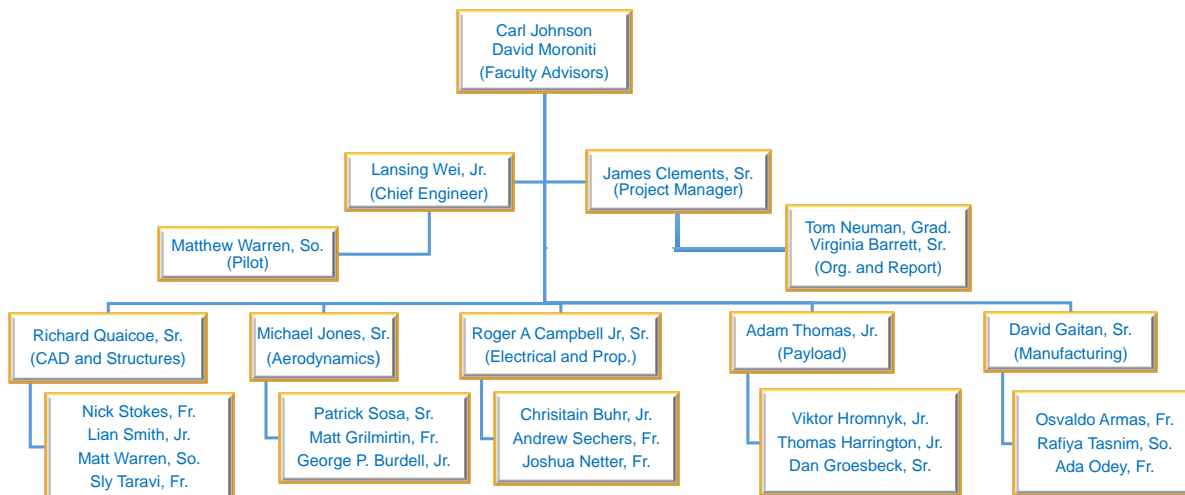


Figure 2.1: Organization chart.

2.2 Milestone Chart

A milestone chart was established at the beginning of the design process to capture major deadlines and design and manufacturing goals. Progress was monitored by team leaders to ensure all major milestones were met. The team worked throughout the entire academic year and established stringent deadlines early to gain testing and flight experience before the competition in April. The team met frequently with the faculty advisors to discuss progress. The milestone chart is shown below in Figure 2.2, capturing planned and actual timing of major events.

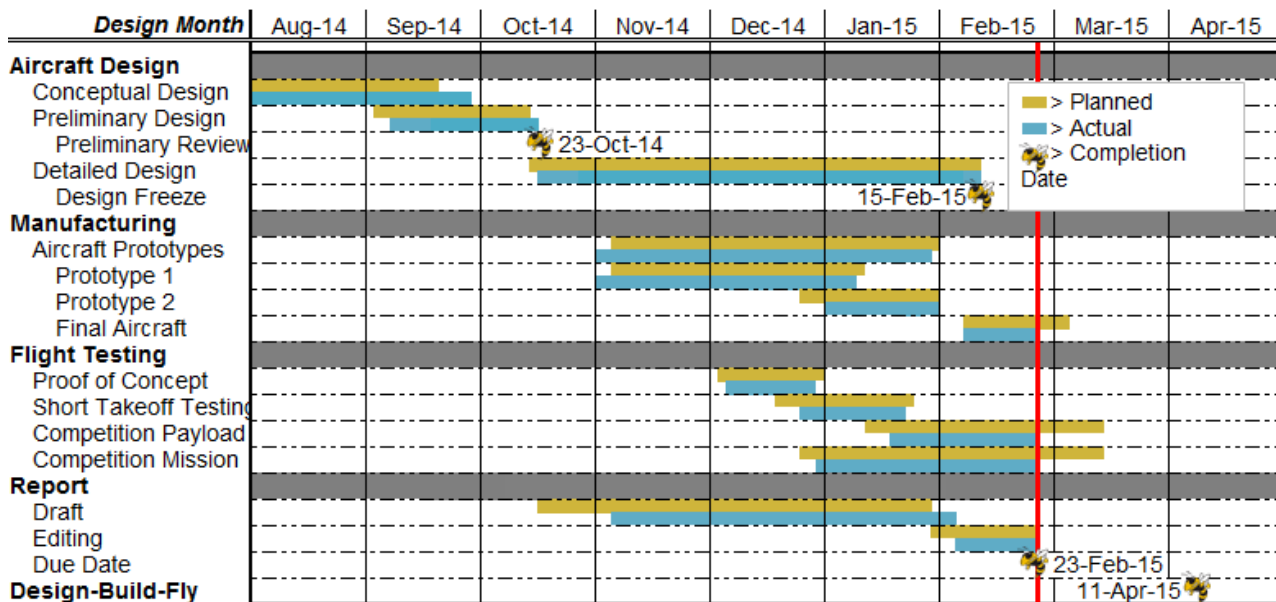


Figure 2.2: Aircraft design milestone chart showing planned and actual objective timings – major deadlines are marked by Buzz, Georgia Tech's mascot.

3. CONCEPTUAL DESIGN

The conceptual design phase was used to evaluate the competition rules, translate them into design metrics, and produce a feasible design configuration that maximized score. The team performed a quantitative scoring analysis in order to pinpoint key scoring drivers. In combination with the mission requirements, characteristics for a successful aircraft were derived. These were translated into Figures of Merit (FOMs), a metric applied to weigh different design choices against each other. The FOMs were applied to a design space of 41,472 possible aircraft configurations and yielded a single conceptual design that *Buzz Killington* is confident will be the best aircraft. The resulting configuration is a conventional airplane with tricycle landing gear, a low wing, and a single engine.

3.1 Mission Requirements

3.1.1 Mission and Score Summary

The AIAA Design/Build/Fly 2014/2015 competition consists of a ground payload loading mission, three flight missions and a design report. The total score for each team is calculated as shown in Equation 3.1:

$$Score = Written\ Report\ Score \times (TMS/RAC) \quad (3.1)$$

Where *TMS* stands for the Total Mission Score from all three missions, calculated using Equation 3.2:



$$TMS = GS \times (M1 + M2 + M3) \quad (3.2)$$

The flight score (FS) is the sum of M1, M2, and M3 scores, which are explained further below. GS is the score gained from payload loading. RAC, or Rated Aircraft Cost, is a term describing the highest empty weight (EW) of the aircraft in any of the flight missions multiplied by the number of servos (N_{servo}) and is seen in Equation 3.3 and Equation 3.4:

$$RAC = EW * N_{servo} \quad (3.3)$$

$$EW = \text{Max}(EW1, EW2, EW3) \quad (3.4)$$

Equations 3.1 through 3.4 show that empty weight and number of servos are the main score drivers, whereas various performance points of the design affect only the flight scores.

The ground mission will take place before any flying mission. The GS is driven by the loading time. For a rapid loading time, the aircraft must have an easily accessible payload bay to load M2 payload as well as a system to quickly accept balls for M3. The loading time is measured in two sections: the time required to load the payload for M2 and secure the aircraft, and the time required to remove the M2 payload and then load the M3 payload. The sum of these sections is the total loading time. The final ground score is the ratio of the fastest loading time in the competition to the loading time of the team, as shown in Equation 3.5. The ground mission must be completed in 5 minutes or a score of 0.2 is used for intermediate scoring calculations. Once the ground mission is completed, the flight missions commence.

$$GS = \begin{cases} 0.2 \text{ if incomplete} \\ \frac{\text{Fastest Loading Time}}{\text{Loading Time}} \text{ If complete} \end{cases} \quad (3.5)$$

All flight missions are flown along the same distance and pattern per lap. For flight missions, the individual portions of the flight pattern seen in Figure 3.1 are as follows:

1. Successful Takeoff within 60 ft.
2. Climb to Safe Altitude
3. 180° U-turn, 500 ft. Upwind from the Start/Finish Line
4. 1000 ft. Downwind
5. 360° Turn Along the Backstretch
6. 180° U-turn
7. 500 ft. Final with a Successful Landing

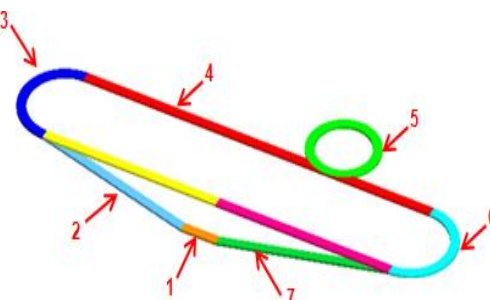


Figure 3.1: Competition flight course.

Each lap is at least 2000 ft. long, or roughly 2500 ft. when accounting for the three turns involved. A complete successful lap is defined as beginning and ending at the start/finish line while still in the air. The required number of laps is defined by the mission.



Mission 1 Ferry Flight: The aircraft must take off within the designated field length and fly as many laps as possible in 4 minutes. Time starts when the aircraft is throttled up and a lap is complete when the aircraft passes the start/finish line. The score is determined by dividing the number of laps for each team by the maximum number of laps completed by any team flying M1 and multiplying by 2, as seen in Equation 3.6:

$$M1 = 2 \times \frac{\text{Number of Laps}}{\text{Maximum Number of Laps}} \quad (3.6)$$

Mission 2 Maximum Load: The aircraft must take off in the designated field length, complete three laps carrying wooden blocks in as little time as possible, and then land successfully. The dimensions and weight of the blocks are detailed in Table 3.1. The blocks are required to be secured to prevent in-flight shift. The scoring of M2 is shown in Equation 3.7:

$$M2 = 4 \times \frac{\text{Fastest Time Flown}}{\text{Time Flown}} \quad (3.7)$$

Table 3.1: Payload composition for Mission 2.

Payload	Size				Number Carried
	Length	Width	Height	Weight (lbs)	
Wooden Blocks	10"	5.5"	1.5"	~1.6	3

Mission 3: Sensor Drop Mission: The aircraft must take off in the designated field length. The external payload is a team-selected number of Champro 12" Plastic Balls. The size and dimensions of the balls are listed in Table 3.2. On each lap, while airborne, the aircraft will remotely drop a single ball. Each drop will occur within a drop zone on the upwind leg of the lap. If more than one ball is dropped in one lap, that lap will be invalidated.

Table 3.2: Payload composition for Mission 3.

Payload	Size				Number Carried
	Length	Width	Height	Weight (lbs)	
12" Champro Balls	3.8"	3.8"	3.8"	~0.1	Team Determined

The score is computed by the number of team laps flown divided by maximum number of laps flown by any team as shown in Equation 3.8:

$$M3 = 6 \times \frac{\text{Number of Laps Flown}}{\text{Maximum Number of Laps Flown}} \quad (3.8)$$



3.1.2 Aircraft Constraints

The competition rules stipulate specific constraints on the aircraft's takeoff distance, propulsion system, and payload:

Takeoff Distance: The aircraft must have the ability to start and take off completely within a 60 foot runway for all three flight missions.

Propulsion System: The aircraft must be propeller driven and electrically powered, with all components of the propulsion system commercially available. These include the motor, propeller, speed controllers, receivers, and batteries. The battery selection is limited to NiCad or NiMH, but may be of any cell count, voltage, or capacity. The entire propulsion battery may weigh no more than 2.0 lbs and must be armed by an external safety plug or fuse. The arming device must be mounted on the exterior of the aircraft and must be accessible from behind in a tractor propeller configuration.

Payload: The aircraft's wooden block payload must be stored internal to the aircraft, and the ball payload must be secured externally and be dropped only due to pilot command. All payloads must be securely fastened to the aircraft's structure so that they do not shift or come loose during flight.

3.1.3 Flight Score Sensitivity Analysis

A sensitivity analysis on the flight scoring drivers was performed to understand the design trades and mission objectives that maximize the flight score (FS) as divided by the empty weight (EW). A conventional sensitivity analysis entails plotting scoring drivers, such as weight or speed, on multiple axes and visualizing the effect on score to determine the maximum. This analysis would show how speed and weight trade in terms of points, and indicate that the aircraft should be as light and fast as possible. In reality, speed and weight are strongly correlated, and it is unlikely for the fastest aircraft to also be the lightest due to a heavy propulsion system. It is also possible for the optimum design to be neither the lightest nor the fastest, but the optimum point is not known when physical aircraft parameters are varied independently. Another deficiency of the conventional scoring analysis is that the team is left to guess the best possible lap count, speed, and ball count for the three missions, since the team's score depends on other aircraft. In all, a conventional scoring analysis does not inform realistic design tradeoffs or scoring goals, therefore, the team sought a more detailed, physics-based approach to the scoring analysis.

Aircraft weight and speed are the main factors that affect flight score, but they cannot be varied independently as described previously. By contrast, aircraft size and propulsion system power are independent design parameters and govern the weight and speed. These two design parameters were varied by two parameters. These two parameters were (1) wing area, assuming a baseline fuselage size required for the M2 payload, and (2) number of battery cells, assuming propulsion power is governed by



the cell count. Aircraft weight and performance were then calculated as functions of the wing area and cell count using the procedure detailed below.

Empty Weight: The aircraft empty weight was divided into propulsion and structural components. The propulsion system weight is proportional to the number of battery cells used. Based on previous team experience, 1,500 mAh NiMH cells were selected as representative batteries, weighing 0.05 lbs each. To fly for four minutes during M1, the average current draw cannot exceed 22 amps without draining the batteries. The electric motor weight was estimated at 0.5 lbs / kW from past experience, and speed controllers that met the pack voltage were cataloged. The propulsion weight assessment is summarized by Equations 3.9-10:

$$P_{electric} = n_{cells} \left(1.2 \frac{V}{cell} \times 20 \text{amps} \right) \quad (3.9)$$

$$W_{propulsion} = n_{cells} \left(0.05 \frac{\text{lbs}}{cell} \right) + P_{electric} \left(0.5 \frac{\text{lbs}}{\text{kW}} \right) + W_{ESC} \quad (3.10)$$

Structural weight was estimated using the team's experience, with a baseline minimum weight which increases with wing area. The coefficients K_A and K_B in Equation 3.11 were adjusted to match past years' Design/Build/Fly planes, and Equation 3.12 summarizes the empty weight assessment:

$$W_{struct} = W_{baseline} + K_A (S_{wing} - S_{baseline})^{K_B} \quad (3.11)$$

$$EW = W_{struct} + W_{propulsion} \quad (3.12)$$

Mission 1 and 2 Speed: The number of laps for M1 and the time to complete 3 laps for M2 were estimated based on the aircraft's maximum velocity and 2,500 ft lap lengths. The maximum speed was calculated using simple power-required calculations that stem from the drag polar, and the power-available from the propulsion system, as seen in Equation 3.13. Lap numbers were truncated down, since only integer numbers of laps count towards the score.

$$P_{req} - P_{av} = \left(\frac{1}{2} \rho V_{max}^3 S C_{D,0} + \frac{2W}{\rho V_{max} S \pi A Re} \right) - P_{electric} \eta_{prop} = 0 \quad (3.13)$$

Mission 2 Takeoff: Aircraft must be able to take off with the 5 lbs payload within 60 ft to receive an M2 score and advance to M3. This constraint was important because it eliminated infeasible designs that have too little wing area or power to take off. The takeoff constraint was solved for a given wing area and power level, with the governing relation shown in Equation 3.14. The K_D term is a function of dissipative forces and wing loading (W/S), while K_T is a function of propulsive forces and thrust loading (T/W).

$$s_g = \frac{1}{2gK_D} + \ln \left(1 + \frac{K_D}{K_T} V_{LO}^2 \right) \leq 60 \text{ feet} \quad (3.14)$$

Mission 3: The number of balls carried for M3 dictates the number of laps flown, since only one ball can be dropped during a single lap. However, the team could not select a number of balls (laps) that would exceed the aircraft's maximum range. It was assumed that the vehicle would operate near maximum L/D to maximize range since there is no time limit for M3. The one-ounce balls were added to the aircraft weight to affect the range and also ensure the aircraft can still take off according to Equation



3.14 above. The propulsion energy available from the batteries dictates the range, so the total energy was calculated from the system efficiency (η) and battery ratings as seen in Equation 3.15. Finally, the maximum number of laps was calculated according to Equation 3.16.

$$E_{av} = \eta_{total} \left[n_{cells} \times 1.2 \frac{V}{cell} \times (0.90_{maximum\ discharge} \times 1500mAh) \right] \quad (3.15)$$

$$Maximum\ M3\ Laps = \frac{E_{av}(L/D)_{max}}{2500ft \times (EW + n_{balls} \times 1oz)} \quad (3.16)$$

The physics-based analysis revealed that neither takeoff nor maximum range constrain the balls to a practical number that could be loaded quickly and fit on the aircraft, so the ball count objective was chosen using the sensitivities in the next report section. This means that the aircraft design point and objectives for M1 and M2 are mostly independent of M3. As a result, the scoring sensitivity in Figure 3.2 below only shows the flight score from M1 and M2 divided by empty weight. The scores seen in the figure depend on the best-performing aircraft resulting from the simulation: 9 laps in M1 and 93 seconds in M2. The plot represents a physics-based tradeoff between speed and aircraft weight, as governed by wing area and battery count.

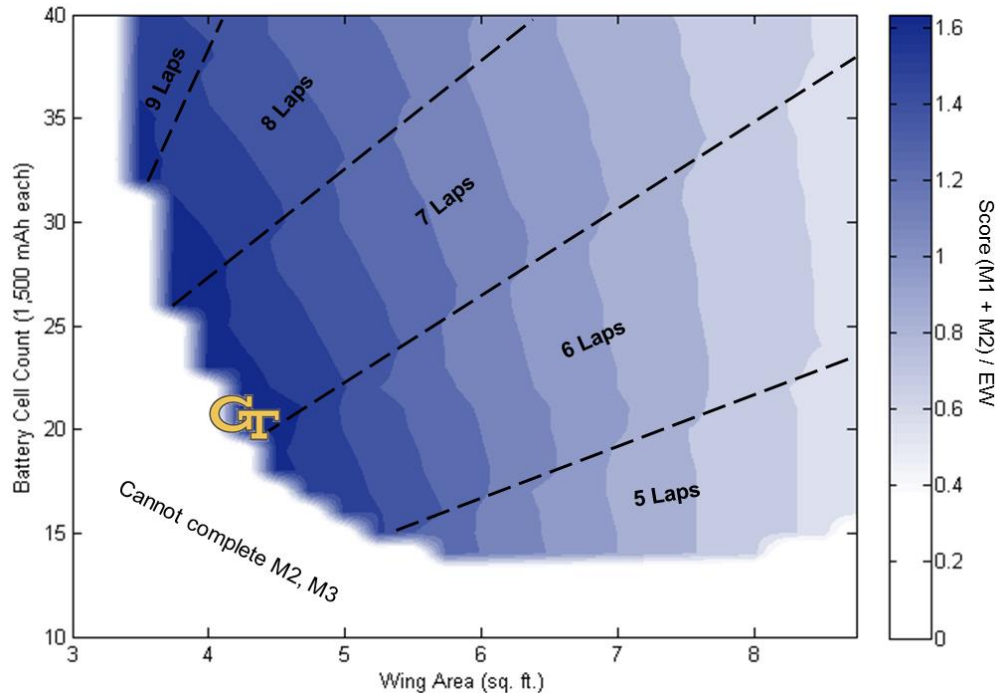


Figure 3.2: A physics-based scoring analysis of the design space for Missions 1 and 2. The team's chosen conceptual design point is noted by the Georgia Tech logo.

Aircraft that could not complete M2 and advance to M3 were assigned a score of zero. In general, smaller and more powerful aircraft are capable of faster flight and thus have higher scores for M1 and M2, but these designs suffer when normalized by EW. Inside of each Lap region, the best-scoring design is



typically the smallest and lightest one and can take off with the M2 payload. Figure 3.2 demonstrates that the highest scoring-potential design must complete 7 laps in M1, have a roughly 2-minute flight in M2, and weigh less than 3 lbs with the best balance of wing area and propulsion system. This was the conceptual design point choice for the team. The optimal design is neither the lightest nor the fastest but represents a good combination of weight and speed, as hypothesized prior to the physics-based analysis.

It should be noted that the analysis performed for this study was simplified, and the boundaries defining laps and ability to complete M2 are not exact. The weight estimates, wing area sizing, and propulsion system selection were also simplified. Therefore, the results were used to realistically assess the scoring space and guide the team's design and objectives, with the aircraft design and sizing pending further refinement and analysis during Preliminary Design.

3.1.4 Ground Score Sensitivity Analysis

The physics-based analysis of the missions indicated that the battery endurance and takeoff do not constrain the number of balls carried in Mission 3. The team decided that a practical volumetric constraint is 10 balls, beyond which the external payload restraint would become too cumbersome and approach the size of the entire aircraft. The best number of balls to carry was determined using two important scoring aspects that could not be modeled in the physics-based method: the number of servos and the loading time.

Number of Servos: The minimum number of servos for safe flight is three: the motor's ESC, the elevator, and either a rudder or ailerons. An additional servo can be added for the payload release mechanism. The addition makes triggering the ball release more straightforward than having to connect a flight servo to the release; however, as the score is divided by the number of servos, the GS would have to be offset by faster loading time.

Loading Time: The loading procedure includes both M2 and M3 payloads. Each payload type has to be loaded and timed separately, with the process also including some time to shuttle back and forth to the aircraft. The team estimated the minimum time for each shuttle and brief loading to be 6 seconds, resulting in a baseline minimum loading time of 12 seconds. Loading time is likely to increase if the team elects to carry more balls, but the additional loading time could be offset by a higher M3 score.

The tradeoff between loading time, number of balls, and number of servos needed to be quantified before significant detail was known about the ball loading mechanism. As a result, the loading time was calculated by simply assigning an average loading time per ball, multiplying by the number of balls, and adding the ball loading time to the baseline time of 12 seconds. The total effect on the score is shown in Figure 3.3 below. The sensitivity analysis shows a distinct break in the scoring at 1.5 seconds per ball: the team should carry as many balls as possible if the average time is faster, or carry only one ball if the



average time is slower. For an equivalent aircraft weight, adding a servo can only be justified if it is 1.0 seconds faster per ball, otherwise the decrease in score is substantial. A quarter-pound increase in the payload mechanism weight can only be justified if it decreases loading time by 0.5 seconds per ball.

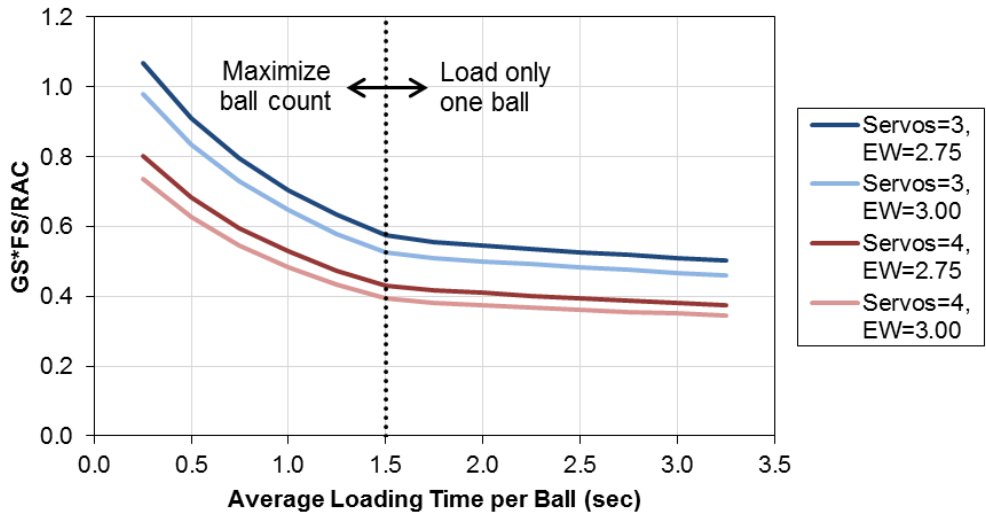


Figure 3.3: The best score obtainable for aircraft with different weights and servo counts, as a function of the average loading time per ball.

Based on this analysis, it was the team's objective to carry as many balls as possible with an average loading time less than 1.5 seconds per ball, without adding a fourth servo, and with the lightest possible external payload support. It can be seen that fast shuttling, M2 loading, and efficient ball loading can nearly double the total score. The loading time and ball capacity for M3 are the top priorities for the team because they constitute approximately two-thirds of the total score. The weight and flight performance for M1 and M2 are lower priorities, but are still critical to fielding a winning design.

3.2 Translation into Design Requirements

The scoring analysis revealed four main components that drive the overall flight score:

Loading Time: Any competitive configuration must be designed for quick loading while withstanding any stresses caused by rapid loading of the wood and balls. In addition the loading device must maximize the external payload without a significant increase in loading time. A balance must be struck between maximum external payload and minimum loading time through testing and engineering judgment.

Servo Count: A servo is defined as any mechanical or electronic device used to control the airplane or payload release mechanism. For the maximum achievable score, the servo count needs to be the absolute minimum number of servos required to control the aircraft and release the M3 payload.



Empty Weight: Any configuration that fails to be as light as possible will not be competitive. Effort must be made to reduce the aircraft empty weight. However, loading time is a critical factor in success. Such considerations must be made carefully to balance loading time and empty weight.

Speed: More flight speed leads to more M1 laps and a lower M2 time. There is also a strong correlation between the number of laps flown in M1 and the number of balls dropped in M3. Both the drag of the configuration and the useful power available via the propulsion system will impact the speed. A balance must be established since increasing power available implies increasing empty weight.

3.3 Configurations Considered

The analysis conducted in Sections 3.1 and 3.2 were translated into qualitative design metrics that were used to evaluate and select an aircraft configuration, as summarized in Table 3.3:

Table 3.3: Rules and requirements translated into design requirements.

Mission/Scoring Requirement	Design Requirement
Minimal Loading Time	High accessibility
Minimal Servo Count	Simple, Robust Design
Low Weight	Efficient Structure
High Speed	Optimized Propulsion

These requirements show that minimizing loading time is the most critical design consideration, followed closely by design simplicity. If a design has the smallest possible loading time and has the least number of servos, it is also likely to have low weight.

After determining the requirements, the next step of conceptual design was establishing a design space that considered all possible aircraft concept configurations. The matrix of alternatives contained five major categories: wings, fuselage, empennage, propulsion, and landing gear. With all component alternatives considered, the design space shown in Table 3.4 contained 41,472 different potential configurations.

Table 3.4: Complete Matrix of Alternatives.

Components	Alternatives			
Wing Layout	Flying Wing	Biplane	Conventional	Tandem Wing
Wing Attachment	Low	Middle	High	Blended
Fuselage Shape	Blended	Rounded	Circular	Square
Number of Fuselages	0	1	2	
Tail Type	V-tail	Conventional	H-Tail	T-Tail
Tail Attachment	One Boom	Two Booms	On Fuselage	
Number of Engines	1	2		
Engine Location	Pusher	Tractor	Both	
Landing Gear	Skids	Tricycle	Taildragger	



3.4 Component Weighting and Selection Process

Figures of Merit (FOM) were created based on the most important configuration factors. The FOM are shown in Table 3.5. The FOMs were assigned an importance of 0 through 5, with 5 being the most important factor and 0 being a non-factor in design.

Table 3.5: Figures of Merit.

Figure of Merit	0	1	2	3	4	5
Mission 2 Accessibility						5
Mission 3 Accessibility						5
Weight					4	
Drag			2			

To reduce the design space from all possible configurations presented in the matrix of alternatives, aircraft components were measured against each other with the relevant FOM. Each configuration was given a scoring value for each figure of merit, and that rating was then multiplied by the FOM value. The scoring values are shown in Table 3.6. The configuration with the highest total quality was then selected for further analysis in the design process.

Table 3.6: Configuration Scoring Values.

Score	Value
1	Inferior
3	Average
5	Superior

3.4.1 Aircraft Configuration

The team examined three basic configurations: a flying wing, a biplane, and a conventional monoplane as shown in Table 3.7.

Table 3.7: Aircraft configuration Figure of Merit.

Aircraft Configurations				
		Conventional	Flying Wing	Biplane
FOM	Value			
Mission 2 Accessibility	5	5	1	1
Mission 3 Accessibility	5	3	1	5
Weight	4	4	1	2
Power	3	4	3	4
Drag	2	4	2	2
Value	20	76	27	54



The biplane was deficient in Mission 2 accessibility due to the top wing interfering with loading the pine blocks. The flying wing was ill suited for either Mission 2 or Mission 3 payloads due to its sensitive C.G. range and short body. The conventional monoplane configuration had the highest total score, and was therefore chosen as the basic configuration for this year's DBF competition.

3.4.2 Wing Placement

Two possible wing locations on the conventional monoplane were considered: a high wing and a low wing. These are shown in Table 3.8, below.

Table 3.8: Wing placement Figure of Merit.

Wing Placement			
FOM	Value	Low Wing	High Wing
Mission 2 Accessibility	5	5	1
Mission 3 Accessibility	5	4	5
Weight	4	4	4
Total	14	61	51

The high wing and low wing configurations both present similar levels of structural efficiency and Mission 3 accessibility. The deciding factor is Mission 2 accessibility. The high wing configuration makes it difficult to maintain a solid wing spar and still load the wooden blocks from the top. As a result, the wing must be placed in a low wing configuration.

3.4.3 Payload Configuration

The ball payload attachment method is critical for reduction of loading time. Three possible locations were considered. The first location was under the wing along the span. However, attaching the payload at this location would increase drag and complicate the release mechanism, reducing speed and increasing loading time. The second location was underneath and along the fuselage. While this location reduces drag, the loading procedure would still be time intensive. The final location considered was on top of the fuselage. This location makes it easy to load while having as low drag as possible and was chosen for these reasons.

3.4.4 Tail Configuration

The ball attachment location above the fuselage could interfere with a conventional T-tail configuration. As a result, the two tail configurations considered were an H-tail and a V-tail, shown in Table 3.9. Both the



H-tail and V-tail move the vertical control surface away from the centerline of the vehicle, minimizing the potential for interference between the vertical surface and the top-mounted M3 payload mechanism.

Table 3.9: Tail Configuration Figure of Merit.

Tail Configuration			
FOM	Value	V-Tail	H-tail
Mission 3 Accessibility	5	5	5
Weight	4	2	5
Total	9	33	45

Selection of a V-tail however requires the use of two servos, one per surface. When considering the requirement for the fewest number of servos, the decision between the empennage choices becomes a choice between Rudder-Elevator and Aileron-Elevator control. Consultation with the team's test pilots indicated that roll control was preferable to yaw control for minimizing lap times. Therefore, the H-tail was selected and would provide elevator control only.

3.4.5 Landing Gear Configuration

The two landing gear options for the chosen wing, tail, and fuselage combination are a tail-dragger configuration and a tricycle configuration as shown in Table 3.10.

Table 3.10: Landing gear configuration Figure of Merit.

Landing Gear Configuration			
FOM	Value	Tail-dragger	Tricycle
Mission 2 Accessibility	5	3	5
Mission 3 Accessibility	5	3	5
Weight	4	5	4
Drag	2	5	3
Total	16	60	72

The tail-dragger is the lighter and has the least drag of the two options, because it allows for minimization of landing gear height. However, this configuration places the aircraft at an angle relative to the ground, which complicates loading procedure and increases loading time. As a result, the tricycle landing gear configuration was chosen.



3.4.6 Propulsion Placement

Since the number of servos includes motors, only one engine was considered. A pusher-mounted motor would interfere with the Mission 3 payload drop. Therefore, a tractor mounting was chosen.

3.5 Final Conceptual Design Configuration

The final configuration is a low wing, H-tail aircraft with a single-engine tractor propulsion system as shown in Figure 3.4. It offers minimum loading time and servo count, while allowing for greater speed by reducing drag. The empty weight of the aircraft is more heavily influenced by structural design, and is discussed later in this report.

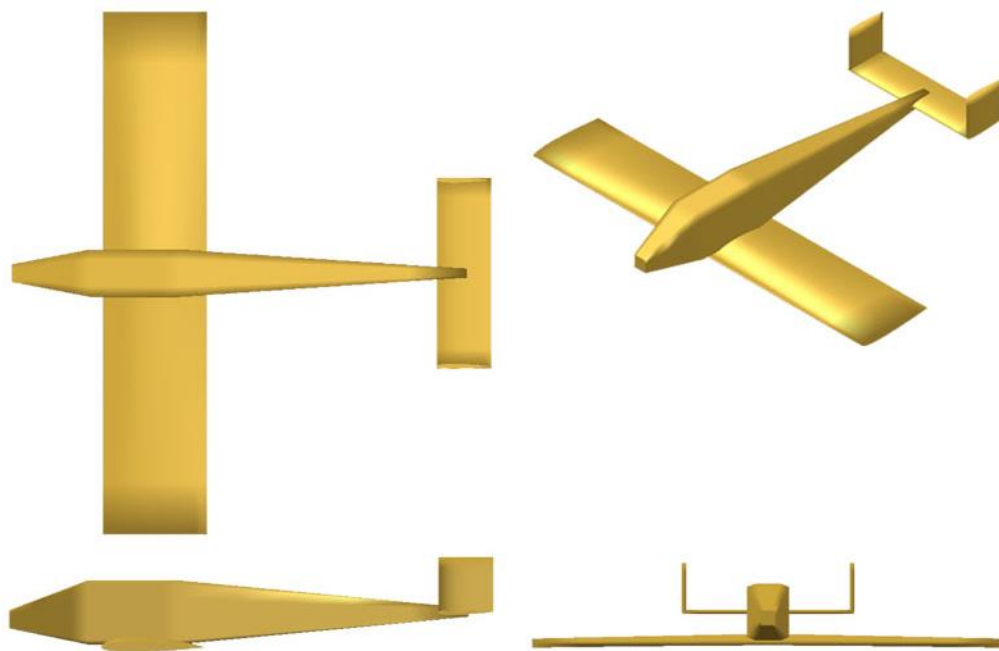


Figure 3.4: Final Configuration.

This configuration used three servos with a predicted empty weight of 2.75 pounds. This corresponds to a RAC score of 8.25. Using the assumed best capabilities of the other aircraft in the competition, this aircraft would be capable of achieving the mission scores tabulated in Table 3.11. Loading time of 1 second per ball and a total loading time of 20 seconds yields a potential TMS of 0.6836.

Table 3.11: Predicted flight scores.

Aircraft	M1	M2	M3
<i>Buzz Killington</i>	7	120	8
Assumed Best	10	96	10
Score	1.4	3.2	4.8



4. PRELIMINARY DESIGN

The objective of the preliminary design phase was to further narrow the design space. To do this, design/sizing trades for the system were evaluated by examining propulsion system options and wing area sizing for takeoff distance. Then weight, drag, motor, propeller and battery data, and aerodynamic coefficients were calculated and combined to estimate mission performance for all three flight missions.

4.1 Design Methodology

The *Buzz Killington* team designed the aircraft configuration using an iterative performance-focused multidisciplinary analysis. The team used constraint sizing to select a weight-normalized design point that could satisfy objectives for all three missions. From this design point, the team analyzed possible propulsion systems, aerodynamic characteristics, built the mission model, and compared them to estimates generated as part of the sizing process. After this analysis, the mission performance and stability of the sized aircraft configuration were computed. The design process detailed in sections below is written as sequential, but iterations occurred throughout, as seen in Figure 4.1. An example of iteration would be updating wing area at a constant wing-loading if propulsion weight is found to be lower, re-evaluating stability and mission performance, and re-adjusting the wing or propulsion system if needed. All iterations were performed with the ultimate goal of maximizing overall score. Therefore, the design shown in this report is the final product of a more complex, iterative procedure.

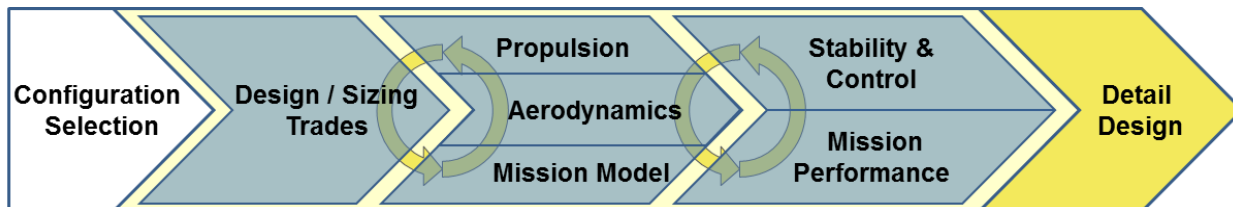


Figure 4.1: The team's preliminary design methodology highlighting multidisciplinary iterations.

4.2 Design Trades

Two trade studies were conducted to determine the size of the aircraft and the propulsion system.

4.2.1 Constraint Sizing

A constraint sizing study allowed the team to analyze the impact of changing wing area, weight, and power required on the various mission parameters to ultimately maximize the total flight score. The trends of Figure 4.2 show that for a given power to weight ratio, increasing wing loading on this graph has three effects: increases the number of achievable laps, decreases the ability to take off, and reduces lifting area. Alternately, increasing power to weight increases the number of achievable laps, increases the ability to take off, and increases the weight of the battery and propulsion system.

The sixty foot takeoff distance requirement gave the first of two lower bounds on the power to weight and wing loading plane. Desired number of laps gave the second lower bound. A takeoff distance of fifty feet



was chosen as a conservative starting point, ensuring that the aircraft would be more than able to meet the sixty feet requirement. This shorter takeoff distance requires a higher power to weight ratio and a higher wing loading. The ideal scoring point will be located close to the intersection of these two bounds without falling below either.

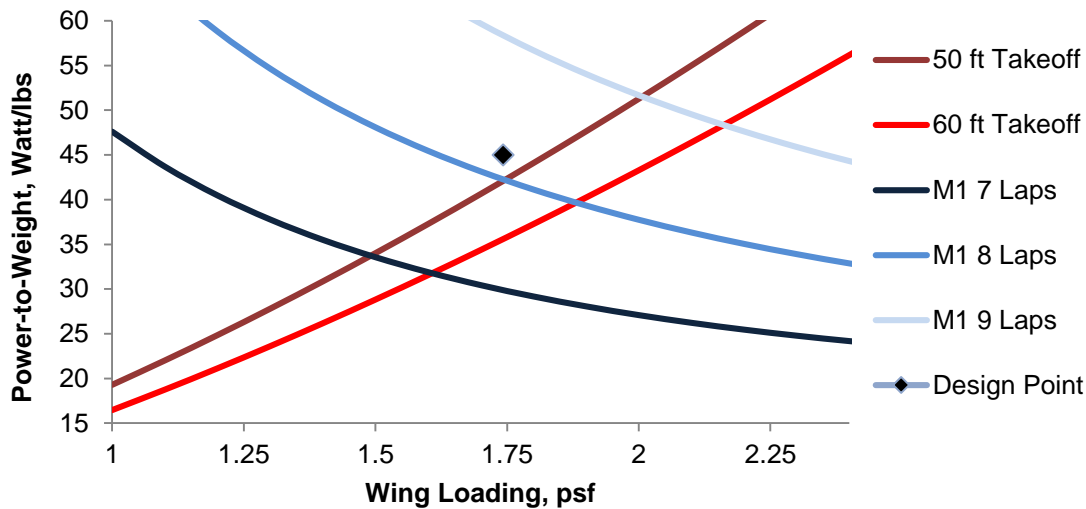


Figure 4.2: Selecting the design point from the constraint plot, marked by the point.

The design point chosen was marked on Figure 4.2. It surpasses the constraint lines for a 50-foot takeoff distance and approximately an 8 lap capability for Mission 1. The point selected has a wing loading of 1.75 psf, and a power to weight of 45 W/lb. Implied in this analysis is an assumption of flying the same number of laps in M3 as M1, since as an endurance-focused M3 can be flown slower to account for higher drag. Next, the impact of the number of laps was analyzed to maximize score. Figure 4.2 shows that the difference between 7 laps and 8 laps is fairly substantial. Choosing 8 laps instead of 7, and thus moving up along the takeoff constraint line, would increase wing loading and the power to weight ratio. The higher weight of the battery and propulsion were chosen to be acceptable because the extra power to weight would add considerable speed to the aircraft during the lightweight M1, as well as increase the performance of the plane during M2.

4.2.2 Propulsion System Selection

The process to select the best motor for the aircraft involved multiple stages. First, a motor database was created subject to several constraints. The motor constant, K_v , was limited to a low value, as a low K_v can drive a larger diameter, more efficient propeller. An upper limit on motor weight of 0.5 lb was chosen to minimize overall empty weight. The database contained over 50 motors from various companies, including Hacker, Tiger, Scorpion, Cobra and AXI.



Next, a propeller database was generated. The propellers were sorted by their pitch to diameter (P/D) ratio. Any propellers with a P/D less than 0.60 were removed from this database. This P/D ratio limit was chosen to ensure that higher thrust levels could be maintained at high speeds. MotoCalc, a commercially available motor analysis tool, was then used to estimate the motor efficiency, static thrust, and thrust at 60 mph for each motor with multiple battery and propeller combinations.

The team sorted the motor, propeller, and battery combinations by weight from least to greatest. The top ten motor combinations were chosen to undergo further testing. The top motor-battery-propeller combinations were analyzed and their variation with speed was graphed. This allowed the team to visualize how various combinations would work under different flight conditions, and to evaluate the most effective combination to meet the competition's needs given the current aircraft's capabilities.

Two motor combinations were chosen to purchase and test, as shown in Table 4.1. The former, although heavier, was selected as the primary motor because it had greater static thrust. However, both motors were purchased and extensively tested to see if the theoretical results would match the actual outcomes. Section 5.3 will go into further detail regarding these tests.

Table 4.1: Final propulsion alternatives.

Motor	Kv	Battery (Cells)	Current (Amps)	Best Propeller	Static Thrust (lb)	Propulsion System Weight (lb)
Tiger 3510-13	700	20 (2,000 mAh)	0.50	11x7	3.81	1.464
Tiger 4010-11	475	20 (1,500 mAh)	0.80	13x10	3.49	1.255

4.3 Mission Model

4.3.1 Description and Capabilities

The three missions were simulated via a set of first order differential equations (Equations 4.1-4.3) defining the position and orientation of the vehicle throughout the flight. By integrating these equations over time using a 4th Order Runge-Kutta approach in MATLAB with some simple logic defining each of the required mission segments, it is possible to define the position, velocity, and orientation of the vehicle over time. The thrust (T) was defined as a function of velocity with the relationship defined by MotoCalc, the analysis tool used in the propulsion system selection. The drag (D) was represented via a parabolic drag relationship. The load factor was explicitly defined for each turn segment, but if it exceeded the estimated maximum lift coefficient, it was limited to that value.

$$\dot{x} = V \quad (4.1)$$

$$\dot{V} = \frac{T - D}{m} \quad (4.2)$$

$$\dot{\psi} = \frac{g\sqrt{n^2 - 1}}{V} \quad (4.3)$$



4.3.2 Uncertainties

The approach described above has specific limitations and uncertainties. The lack of a vertical dimension means that it cannot capture any aerodynamic effect due to altitude changes, or for the energy required or saved due to climbing or diving. The lack of any wind model discounts any additional drag due to sideslip in flight, or changes in velocity depending on traveling with or against the wind. The flight path defined for each lap assumes an idealized flight path, with the pilot turning perfectly after each 1000 ft. leg and the turns being optimal turns. Finally, there are additional uncertainties in the mission predictions due to any errors or inaccuracies in the thrust and drag predictions.

4.4 Aerodynamic Characteristics

4.4.1 Airfoil Selection

Using the correct airfoil for the aircraft is key to achieve the aerodynamic characteristics required to compete in this competition. Hundreds of airfoils were analyzed through a MATLAB script at an estimated Reynolds number of 200,000 to choose an airfoil that could provide the requisite lift and moment coefficients. These airfoils were also filtered based on their thickness and manufacturability.

Manufacturability: Complex airfoil geometry, as shown in Figure 4.3, can result in manufacturing error. These imperfections can negatively impact the aerodynamics of the vehicle and therefore its performance. The airfoil must not have a highly cambered or sharp trailing edge while maintaining sufficient thickness to reduce these manufacturing difficulties and obtain the desired performance from an airfoil.

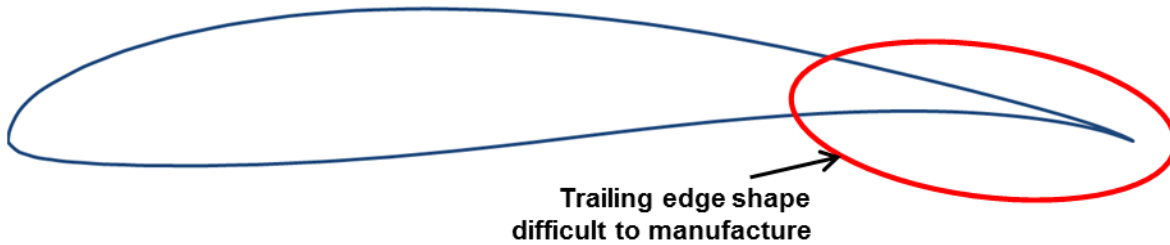


Figure 4.3: Wortmann FX 63-137 showing poor manufacturability.

Thickness: Low thickness airfoils typically have a small leading edge radius that results in abrupt stall at lower angles of attack. Increasing airfoil thickness increases the space for internal structural members that increase the structural rigidity of the airfoil while reducing structural weight. After testing multiple airfoil types, a thickness greater than 12% was preferred to achieve the space for these members.

Afterwards, the filtered airfoils were further analyzed based on maximum section lift coefficient and lift to drag ratio. Drag and lift curves for the final four airfoils were constructed using airfoil data obtained from wind tunnel test results from UIUC as shown in Figure 4.4.

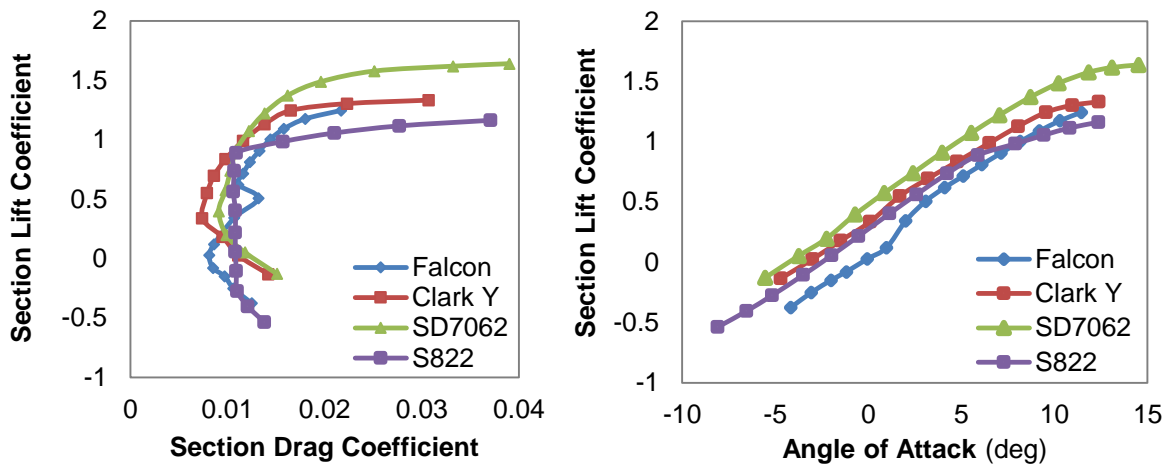


Figure 4.4: Experimental lift and drag characteristics for selected airfoils from UIUC data.

Examination of the drag polar shows that the SD7062 and S822 airfoils have a more stable sectional drag coefficient (\bar{C}_D) over longer ranges of \bar{C}_L than the other airfoils. This indicates that for a given range of \bar{C}_L values, namely those around a \bar{C}_L of 0.5, the \bar{C}_D remains relatively low and constant. This is important due to the variance of \bar{C}_L over the wings caused by downwash due to wingtip vortices and environmental variables such as local wind. A high maximum \bar{C}_L is a desirable airfoil characteristic as it enables good STOL performance, which is critical due to the sixty foot takeoff requirement.

The SD7062, shown in Figure 4.5, has a thickness to chord ratio of 14% which aids in both the manufacturing process and increases the geometric stiffness of the wing. The SD7062 also had a maximum \bar{C}_L and lift-to-drag higher than the other airfoils considered, enabling the team to select the best combination of takeoff performance and speed. In summary, the SD7062 airfoil was selected for its combination of high maximum \bar{C}_L , manufacturability, thickness to chord ratio, and favorable lift to drag ratio.



Figure 4.5: SD7062, the team's selected airfoil.

4.4.2 Lifting Surface Analysis

Athena Vortex Lattice (AVL), an aerodynamic tool developed by Dr. Mark Drela at MIT, was used to model the lifting surfaces of the aircraft to compute the aerodynamic characteristics of the entire aircraft. AVL models lifting surfaces as an infinitely thin sheet of discrete vortices, and models their interactions. The aircraft's tail and control surfaces were sized in AVL to provide desired static stability and trim characteristics. The aircraft configuration and paneling in AVL is seen in Figure 4.6. The lift distribution



shown in Figure 4.7 was generated in AVL using elevator trim to maintain flight at a moderate angle of attack on approach and landing. Due to the distribution shape, stall is expected to occur at the wing root, allowing the pilot to maintain roll control using the ailerons that are mounted outboard.

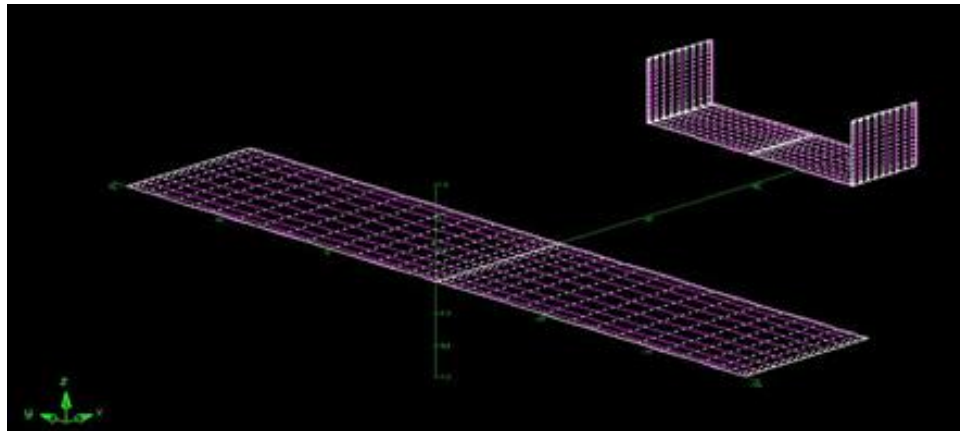


Figure 4.6: AVL model of aircraft.

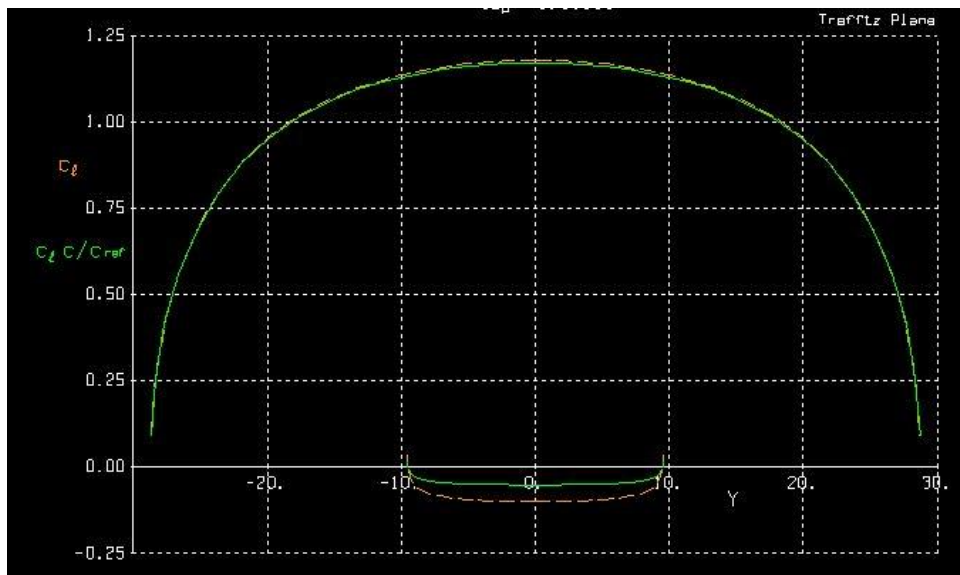


Figure 4.7: AVL predicted lift distribution of the aircraft.



4.4.3 Drag Analysis

A preliminary parasitic drag estimate was computed by summing each component's drag contributions, approximated using the semi-empirical methods from Hoerner's *Fluid Dynamic Drag*, and then normalizing each component according to the wing reference area. Table 4.2 shows the contributions of the main aircraft components, with Figure 4.8 displaying the same data as a percentage breakdown.

Table 4.2: Aircraft zero lift drag estimates.

Component	$C_{D,0}$
Wing	0.0137
Landing Gear	0.0085
Payload Release	0.0064
Fuselage	0.0059
Tail	0.0013
Total	0.0358

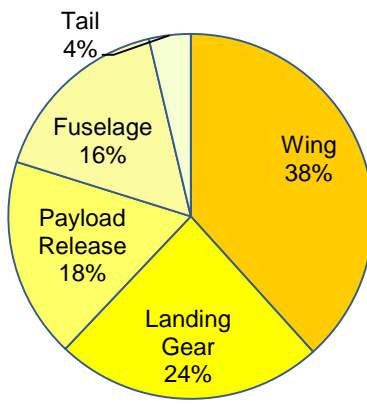


Figure 4.8: Graphical representation of drag estimates.

The main components of the parasitic drag are detailed below:

Wing: The drag coefficient for the wing was calculated using Equation 4.4 from Hoerner:

$$C_{D,0} = R_{wf} R_{LS} C_{fw} \left(1 + L' (t/c) + 100 (t/c)^4 \right) \cdot \frac{S_{wetw}}{S} \quad (4.4)$$

Equation 4.4 contains terms correcting for wing thickness location, sweep, and wing-fuselage interference (L' , R_{LS} , and R_{wf} , respectively). The flat-plate skin friction coefficient (C_f) is a function of Reynolds number approximated for fully turbulent flow. The wing was found to be the largest contributor to zero-lift drag, with a total $C_{D,0}$ contribution of 0.0137, which is about 38% of the total drag.

Landing Gear: The landing gear components are significant contributors to the overall drag of the aircraft. The main gear and nose gear drag contributions were calculated separately, but both were modeled as a wheel and a flat plate added for the strut. The overall contribution of the landing gear to the drag was about 24%.

Payload Release: The drop mechanism significantly increased the overall drag of the aircraft. The drag of the drop mechanism was modeled as a flat plate, with a wedge nose to reduce drag. Knowing the relation between drag of a wedge compared to a flat plate, the zero-lift drag contribution was found to be 0.0064, or 18% of the overall drag.

Fuselage: The drag coefficient for the fuselage was determined using Hoerner's method, which computes drag as a function of the body fineness ratio, the Reynold-adjusted skin friction coefficient, and



lifting-surface/fuselage interference. The total $C_{D,0}$ contribution by the fuselage was calculated to be 0.0059, which accounted for about 16% of the drag.

Tail: The tail surfaces were modeled as wings and the drag contributions were calculated using the same method as the wing calculation. Overall, the contribution of the tail to the drag was 4% due to their small size.

With parasitic drag computed, the team used AVL to model the lifting surfaces of the aircraft to estimate induced drag. The estimated span efficiency was 80% for the full configuration. Sub-optimal efficiency was preferred to manufacturing complexity added by sweeping, twisting, or tapering the wing. The full drag polar is displayed in Figure 4.9 and was calculated by adding the induced drag from AVL and the parasitic drag from above. The drag polar indicated lift-to-drag ratios around 8 for the majority of lift coefficients, a relatively low value that can be attributed to the large fuselage driven by Mission 2 and 3 payload volume.

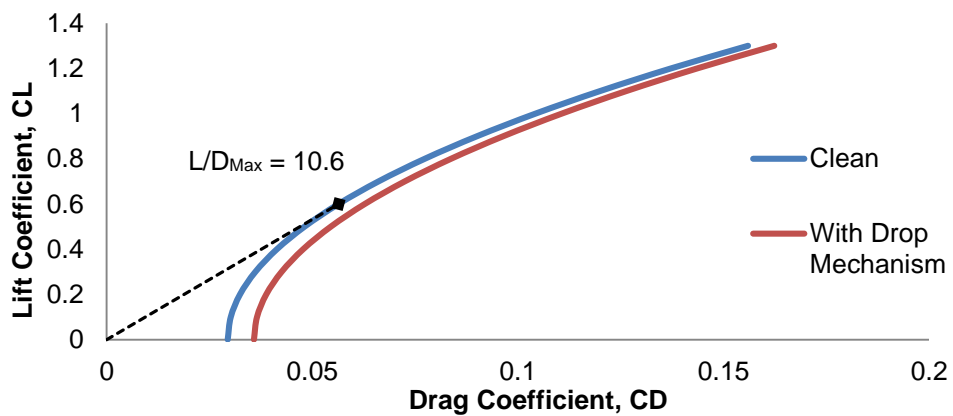


Figure 4.9: Full drag polar.

4.5 Stability and Control

Static and dynamic stability were analyzed to ensure that the aircraft would be able to successfully complete the flight missions. The fastest speeds, slowest speeds, heaviest weights, lightest weights, cruise, climbs, and turns were all considered, with results presented only for the critical flight condition.

4.5.1 Static Stability Analysis

Static stability was evaluated using the vortex lattice method implemented in AVL. The most demanding flight condition for trim was at the highest weight and lowest speed in Mission 2. Stability derivatives are given for this flight condition in Table 4.3. The aircraft is trimmed at this condition with a small elevator deflection and no extreme deflections were required for any of the cases analyzed. All cases indicate the aircraft is longitudinally, statically stable with a static margin of 9.3%. All pitch, roll, and yaw derivatives are stable and within the acceptable range based on previous years' pilot feedback.



Table 4.3: Relevant stability coefficients and derivatives for static stability.

Parameter	AVL Results	
Inputs	W_{total} (lbs.)	8.0
	V (ft/s)	35.3
Aerodynamic Parameters	C_L	0.97
	α (deg.)	10.0
	β (deg.)	0.0
Deflections	$\delta_{elevator}$ (deg)	-8.9
	$\delta_{aileron}$ (deg)	0.0
Stability Derivatives	$C_{l,\beta}$ (rad $^{-1}$)	-0.13
	$C_{L,\alpha}$ (rad $^{-1}$)	4.04
	$C_{m,\alpha}$ (rad $^{-1}$)	-0.38
	$C_{n,\beta}$ (rad $^{-1}$)	0.11
Damping Derivatives	$C_{l,p}$ (rad $^{-1}$)	-0.37
	$C_{m,q}$ (rad $^{-1}$)	-7.35
	$C_{n,r}$ (rad $^{-1}$)	-0.077
Static Margin	% Chord	9.3

4.5.2 Dynamic Stability Analysis

Knowing the trim conditions from the static stability analysis, the next step was to use the aerodynamic derivatives about the trim conditions to investigate the dynamic behavior of the airplane. The stability and control derivatives were obtained using AVL, the mass properties were obtained from the CAD file, and the stability characteristics were calculated using the six degrees of freedom linearized differential equation matrix found in Phillips' *Mechanics of Flight*, Section 9.8. The eigenvalues and eigenvectors of the matrix revealed that the aircraft is stable in the Short Period, Dutch Roll, and Roll modes, unstable in Spiral mode, and neutrally stable in Phugoid mode. The Spiral mode has a 4.2 second doubling time, which is in line with past year's airplanes that flew without issue. The flight conditions used for this calculation were the same ones used in the static stability section, listed in Table 4.3. The dynamic stability characteristics are tabulated in Table 4.4.

Table 4.4: Dynamic stability analysis for least stable case.

	Longitudinal Modes		Lateral Modes		
Mode	Short Period	Phugoid	Dutch Roll	Roll	Spiral
Damping Rate (s $^{-1}$)	4.00	-0.053	0.62	8.46	-0.16
Time to double/half (s)	0.17	13.03	1.10	0.08	4.17
Damping Ratio (~)	0.72	-0.061	0.13	-	-
Damped Natural Frequency (s $^{-1}$)	3.88	0.87	4.66	-	-
Undamped Natural Frequency (s $^{-1}$)	5.57	0.87	4.70	-	-



4.6 Mission Performance

The lap trajectory was calculated using the mission simulation described in Section 4.3 in conjunction with propulsion characteristics from MotoCalc and aerodynamic characteristics of the airplane. The velocity profile for the first lap of Mission 1 using an 11x7 propeller and a Tiger MN 3510-13 motor is shown on the left of Figure 4.10, and the profile for M2 also using an 11x7 propeller and Tiger MN 3510-13 is shown on the right of Figure 4.10. Both figures show the first lap of each mission and include the initial acceleration after takeoff. Velocity deficits in the plots correspond to the required turns over the course of each lap. The maximum velocity estimated for M1 is 70.0 mph (102.7 ft/s), and the maximum velocity for M2 is 63.3 mph (92.8 ft/s). The estimated lap times using optimal propellers for each mission are shown in Table 4.5, and correspond to a lap started and finished in the air. The analysis indicates that M1 and M2 performance targets of 8 laps and 120-second flight time, respectively, are achievable. It should be noted again that the analysis is likely optimistic, as detailed in Section 4.3, and true lap times will be verified through flight testing.

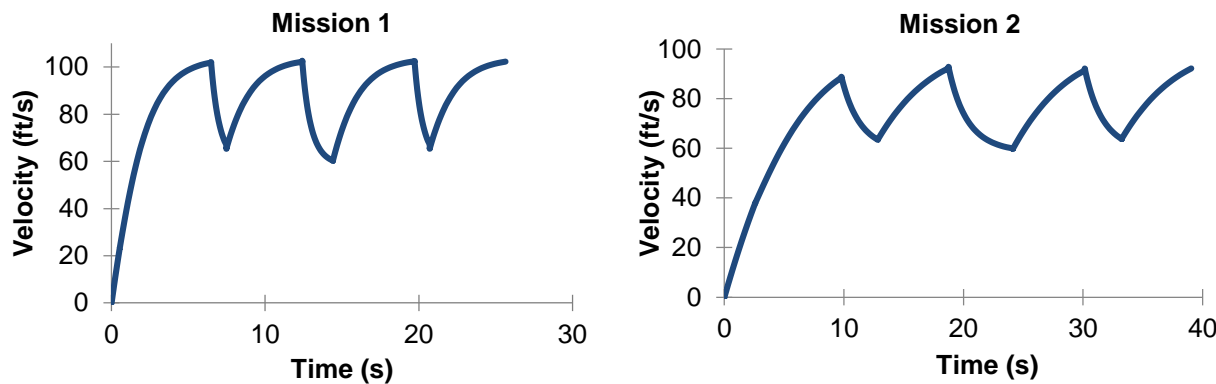


Figure 4.10: Simulation of Mission 1 and 2 lap trajectory.

Table 4.5: Predicted mission performance for each mission-propeller combination.

Mission	Propeller	Lap Time(s)
M1	11x7	25.6
M2	11x7	39.1

5. DETAIL DESIGN

5.1 Final Design

The aircraft dimensions did not vary between the preliminary and detailed design stages because the structural analysis and layout, component selection, and weight-balance calculations did not indicate major changes were needed. With the sizing completed, the final dimensional parameters are listed in Table 5.1. All wing and control surface chords were chosen to allow sufficient thickness for structure and embedded servos, and then sized to provide stability at the constraint-derived wing area, leaving aspect



ratio as a fallout variable. In summary, the final aircraft was designed for flight stability, simplicity, and structural efficiency.

Table 5.1: Final aircraft dimensional parameters.

Overall Dimensions			Wing		
Length	49	in.	Span	57.5	in.
Wing L.E. X-Location	10.7	in.	Mean Chord	11.5	in.
C. G. X-Location	12	in.	Aspect Ratio	5	~
Static Margin	9.3%	chord	Wing Area	661.25	in. ²

Horizontal Tail			Vertical Tail (x2)		
Span	19	in.	Span	5	in.
Chord	6	in.	Chord	6	in.
δ_e, max	30	deg.	δ_r, max	0	deg.
Reference Area	114	in. ²	Reference Area	30	in. ²

5.2 Structural Characteristics

5.2.1 Layout and Design

The primary goal for the structural layout was to ensure that all loads were accounted for and have an adequate load path to the major load-bearing components. The team divided all the loads the aircraft would see into three categories:

Motor Loads: Includes thrust, torque, and sustained vibrations. Components should be made of harder, quasi-isotropic materials such as plywood, and all fasteners must be locked.

Aerodynamic Loads: Includes wing and control-surface lift, drag, and moment, which translate to bending and torsion. Components can be anisotropic for added strength in the load direction.

Ground Loads: Includes aircraft weight and landing impact. Struts should be metal, which sustains impact by bending, not breaking.

The loads on the aircraft need to transfer into the major load bearing components, which includes the wing spar and fuselage attachment point. In flight, the wing may sustain up to a 2.5g load at maximum weight, based on the requirement of the wing tip test, therefore all loads from components not on the wing, such as payload and the empennage, traverse to the spar attachment point via the fuselage, as demonstrated in Figure 5.1. The fuselage is geometrically stiff due to the size required to accommodate the payload, making it an adequate load path. For the ground loads the fuselage has hard-points at the gear attachment locations to ensure impact loads do not damage any components.

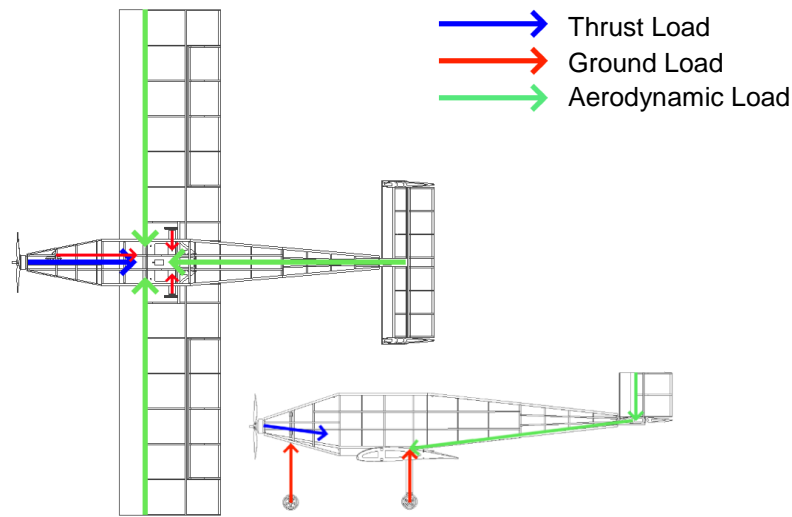


Figure 5.1: Load paths of major forces.

5.2.2 Operating Envelope

With the loads mapped and layout complete, the structure of the airplane was designed to withstand the design load of 2.5g at the maximum gross weight of 8 lbs. This translates to a 66-degree bank angle for sustained level turns. The ultimate load could not be well quantified because balsawood has significant variation in ultimate strength, thus the 2.5g design load-limit at small deflections was retained as the maximum positive load envelope for Mission 2. Since M1 and M3 fly at lower weights than M2, the structural limit increases to 6.25g. The negative load limit was defined at -1g for M2 to prevent the wing attachment area from failing in compressive buckling. This translated to greater negative loads for M1 and M3 due to their load limits. The defining structural limits were combined with aerodynamic performance limits at each mission to construct the V-n diagram displayed in Figure 5.2.

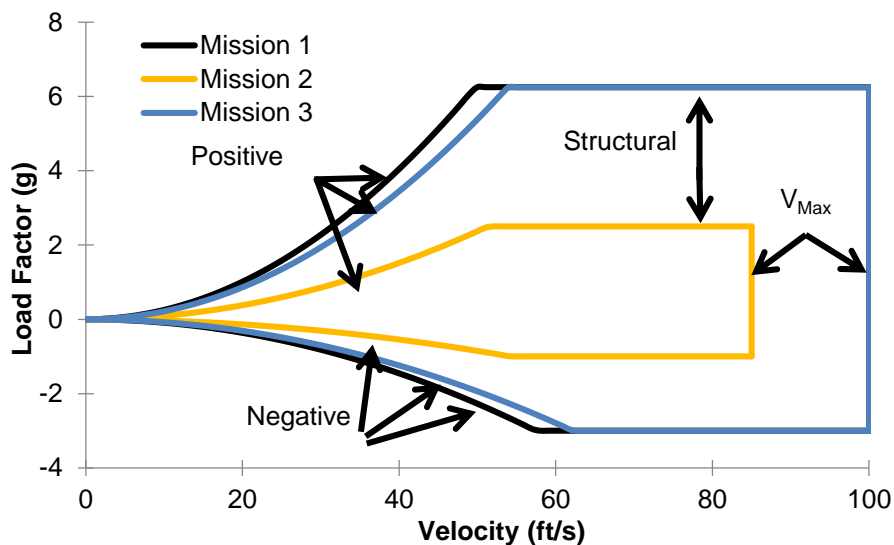


Figure 5.2: V-n Diagram showing loading as a function of velocity for Missions 1, 2 and 3.



5.3 System and Subsystem Design/Component/Selection/Integration

To finalize the aircraft design, the following subsystems were analyzed with greater detail: radio controller, servos, main wing, propulsion system, landing gear, and the structural architecture/assembly for each of these components.

5.3.1 Fuselage/Payload Bay

The fuselage of the aircraft is of a bulkhead and stringer design, using balsa wood for the majority of the structural members, with plywood being used to reinforce critical areas. The geometry of the fuselage design was primarily driven by enclosing an internal payload bay that could contain the payload for Mission 2. This led the team to design around the volume and weight requirements for the five pound payload block with a single open volume for the entire payload. Bulkhead placement was based on providing structural support to the payloads.

The CAD model was developed such that the bulkheads had interlocking slots, so that the parts fit together like a jigsaw. This interlocking method allows for the grain direction of the balsa wood to be in the proper direction for load transfer and more efficient manufacturing. The interior of the fuselage is open to allow for free arranging of the payload, the batteries, receivers, controllers and wires for the electronic components.

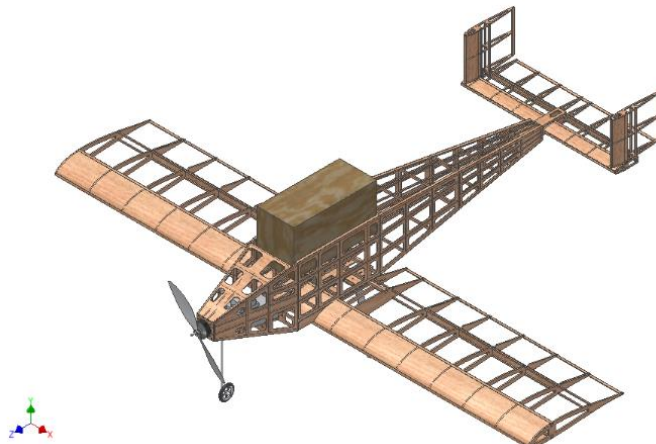


Figure 5.3: Payload loading method.

The fuselage was designed with a top lid that can easily open to allow rapid and simple access to the payload, and to provide a solid base to mount the payload drop mechanism for Mission 3. This is shown in Figure 5.3.



5.3.2 Wing

The wings were designed in a conventional scheme, with a rib and spar layout. The main load bearing structure was a balsa spar located at the quarter chord, which was reinforced with carbon fiber flat rectangular rods, and supplemented with an aft spar located at the three-quarter chord for the aileron attachment, as shown in Figure 5.4. Balsa wood was selected as the material for the spars and ribs, due to the strength, weight, and ease of manufacturability.

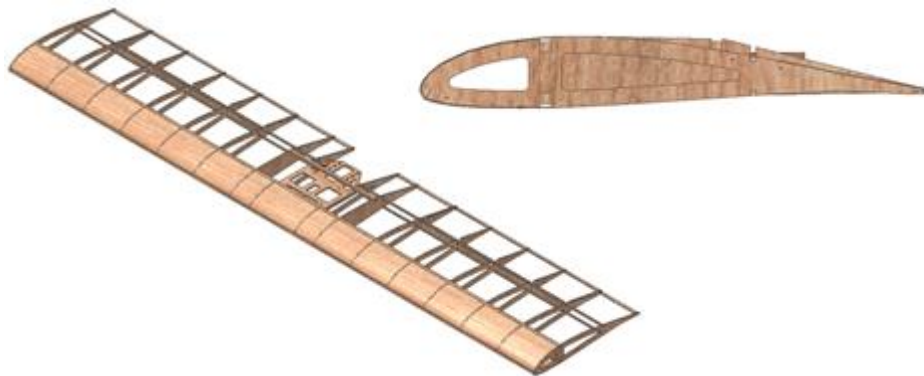


Figure 5.4: Wing design and structural layout.

The middle of the wing was designed around a central plate that integrated the aileron servo as well as acting as the attachment point to the main fuselage. The servo was connected to push rods and control horns to move both ailerons, which were then attached along the aft spar of the wing. Several ribs were modified to allow these push rods to pass from the center of the plane out into the wings. The hinges of the ailerons were fabric hinges, which are both small and lightweight.

5.3.3 Motor Mount

In keeping with the team design goal of minimizing system weight to maximize overall score, the motor mount is connected directly to the front section of the main fuselage. The motor attaches directly to a plate of 1/8th inch thick poplar plywood, shown in Figure 5.5, which was selected for its ability to withstand the torque and static thrust of the motor.

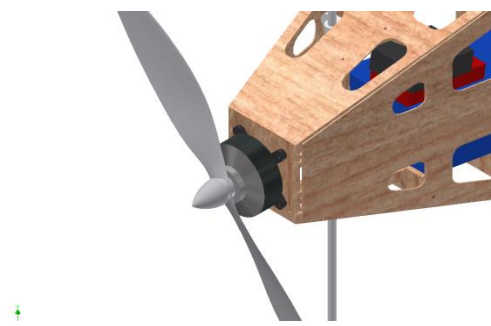


Figure 5.5: Motor mount assembly.



5.3.4 Empennage

The empennage, seen in Figure 5.6, was designed in CAD to be a lightweight and effective control surface. The construction uses similar materials and construction techniques as the wings, with balsa wood used for the majority of the structure, augmented by plywood members in key locations.

The tail was constructed as a separate unit from the fuselage and was attached to the aft of the fuselage with a box that fit into the back two bulkheads on the fuselage. This would allow removal and replacement of the tail, as new iterations of the tail or modifications were made. Wiring for the control servos runs through the tail box and into the fuselage.

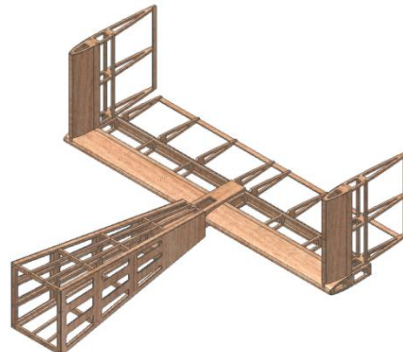


Figure 5.6: Empennage assembly.

In addition to providing stability and control authority in flight, the tail also supports part of the ball drop mechanism, which is connected to the elevator to allow commanded ball drops to avoid the added complexity, weight, and RAC of a dedicated drop servo.

5.3.5 Ball Deployment Mechanism

The ball deployment mechanism system was designed to reliably deploy the balls for Mission 3 without performing a maneuver dangerous to the aircraft or requiring an additional servo. This system consists of a series of 3D printed shuttles which slide along carbon fiber rods mounted to the top of the aircraft. A small lever arm placed near the tail of the aircraft uses the elevator servo to force the ball off the shuttle and away from the aircraft. The mounted deployment mechanism is shown in Figure 5.7.

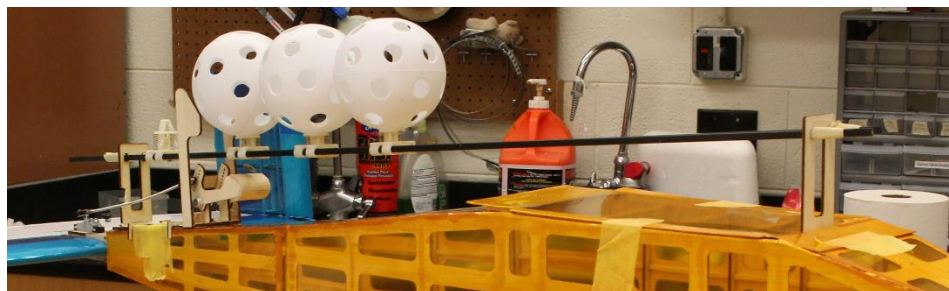


Figure 5.7: Ball deployment mechanism.



The 3D-printed shuttle was designed to hold the balls in place utilizing three linked arms that fit into one of the holes in the ball. A set of springs is compressed during the loading procedure, locking the arms into an extended position which locks the ball in place. A lever connected to the aircraft's elevator pushes a pin underneath the carriage which contracts these arms and releases the ball. The lever is connected to the elevator such that an elevator deflection above 35 degrees will force the lever arm to push the pin. Normal flight would not require an angle of 35 degrees preventing a premature ball release. The drag acting on the unreleased balls forces them to slide back onto the release arm after a drop, effectively reloading the mechanism.

The system works in a binary manner; the balls are either released or not. This increases the system reliability, as the transmitter can be set to limit servo travel during the lap to be below the deployment threshold, until the pilot flips a switch and enables full travel. Below are images of the ball holder and lever devices in Figure 5.8.

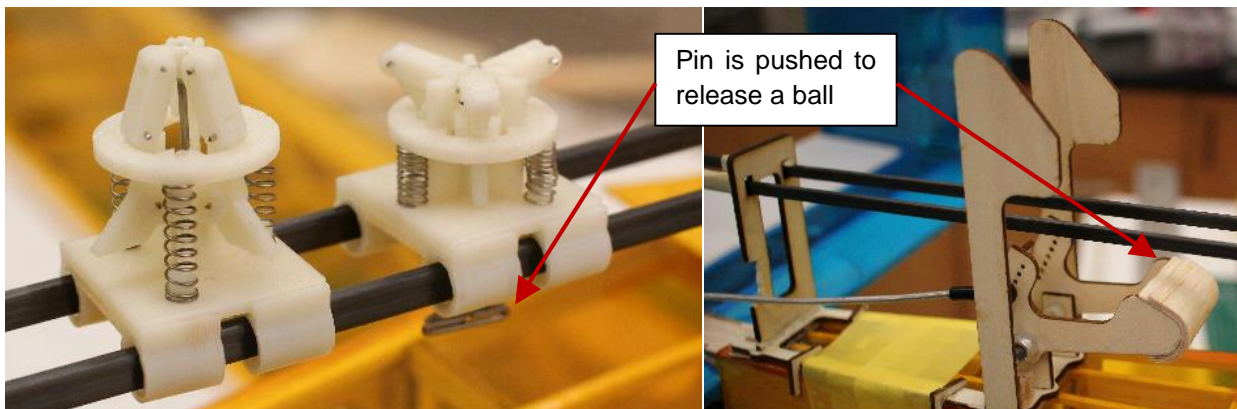


Figure 5.8: The shuttle for the drop mechanism and the lever system.

5.3.6 Receiver and Transmitter Selection

The receiver selected is the Futaba R6008HS, as it provides the required failsafe mechanism with minimum weight. *Buzz Killington* used a Futaba T8FG 2.4 GHz radio transmitter to communicate with the Futaba receiver.

5.3.7 Propulsion System

The propulsion system components were initially selected using the analysis from the MotoCalc program, as described in Section 4, but were changed after the results of wind tunnel testing described in Section 7 and 8. Originally, the Tiger MN 3510-13 motor was selected, but based on the data described in Section 8, it was found that the initial motor thrust was over predicted and that the Tiger MN 4010-11 was a better choice. The final selected propulsion system consists of a Tiger MN 4010-11 motor, 20 cell Elite 1500 mAH NiMH battery pack, a Phoenix Edge Lite 50 speed controller, and different propellers for each mission. The chosen propellers are APC 12x10 for Missions 1 and 3 and APC 13x10 for Mission 2.



5.3.8 Servo Selection and Integration

The Turnigy 380MAX was selected as the servo for the aileron and nose-gear as well as the servo for elevator and release mechanism. These servos were selected by analyzing hinge-moments for each control surface using AVL and then finding servos that had sufficient control power to handle the calculated moments, with the lightest weight possible. The selected components are tabulated in Table 5.2:

Table 5.2: Selected components.

Components	Description
Motor	Tiger MN 4010-11
Battery	20 cell ELITE 1500
Speed Controller	Phoenix Edge Lite 50
Receiver	Futaba R6008HS
Transmitter	Futaba T8FG
Aileron and Nosegear Servo	Turnigy 380MAX
Elevator and Release Servo	Turnigy 380MAX

5.4 Weight and Balance

An important aspect of stability is correct center of gravity (C.G.) measurements. To measure the C.G., a simple calculator was created that consisted of a list of all components, their weights, and their locations along the x-axis and z-axis. Component weights were first estimated using the CAD model and then confirmed with the physical vehicle. The results for all scenarios are given in Table 5.3. The x-axis was measured positive aft of the nose of the aircraft and the z-axis was measured positive above the chord-line of the wing. The predicted C.G. location from the CAD is shown in Figure 5.9.

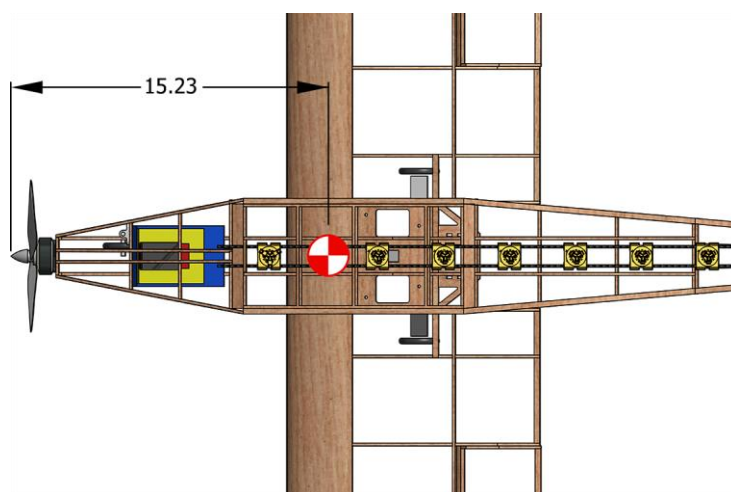


Figure 5.9: C.G. location on CAD model.



Table 5.3: Weight and balance chart.

Empty Weight					
Component	Weight (lbs)	C.G. loc.(in, x-axis)	Moment (in-lbs, x-axis)	C.G. loc. (in, z-axis)	Moment (in-lbs, z-axis)
Fuselage	0.18	18.00	3.28	2.00	0.36
Empennage	0.11	44.00	4.77	4.00	0.43
Speed Controllers	0.02	8.00	0.16	2.13	0.04
Receiver	0.03	3.00	0.09	2.13	0.06
Propeller	0.04	1.00	0.04	3.75	0.15
Wing	0.49	18.00	8.91	0.00	0.00
Aileron Servo	0.04	18.00	0.72	1.50	0.06
Tail Servo	0.04	45.00	1.80	4.13	0.17
Main Gear	0.19	19.50	3.66	-4.00	-0.75
Nose Gear	0.06	6.00	0.33	-3.50	-0.19
Motor	0.24	3.00	0.73	3.75	0.91
Receiver Battery	0.28	6.00	1.65	1.75	0.48
Aircraft Totals	1.72	15.23	26.15	0.99	1.73
Mission 1					
Battery	1.36	15.00	20.35	2.00	2.71
Payload	0.00	0.00	0.00	0.00	0.00
Aircraft Totals	3.07	15.13	46.49	1.45	4.44
Mission 2					
Battery	1.36	8.00	10.85	2.00	2.71
Payload	5.00	16.00	80.00	4.00	20.00
Aircraft Totals	8.07	14.49	117.00	3.03	24.44
Mission 3					
Battery	1.36	6.00	8.14	2.00	2.71
Payload	0.52	38.00	19.69	4.00	2.07
Aircraft Totals	3.59	15.03	53.98	1.81	6.52

The table shows that the battery must move significantly in order to balance C.G. for each mission. This is non-ideal, but necessary due to the large change in the nature of the payloads between Mission 2 and Mission 3.

5.5 Flight and Mission Performance

5.5.1 Flight Performance

The flight performance of the aircraft may be described by the point performance of the vehicle. Key aspects include the velocity envelope and turn performance, as well as takeoff distance and stall speed. These are given below in Table 5.4.



Table 5.4: Aircraft flight performance parameters for each mission.

	Mission 1	Mission 2	Mission 3
Weight (lb.)	3.07	8.07	3.59
W/S (psf)	0.653	1.742	0.828
TOFL	6.72	53.2	10.76
V_{stall} (ft/sec)	21.93	35.80	24.06
V_{max} (ft/sec)	95.0	81.78	93.0
Load Factor	6.67	2.5	6.5
Turn Radius (ft.)	42.52	90.65	17.2
Time for 360° (s)	3.49	7.45	3.03

Weight represents the Mission 1, 2, and 3 gross take-off weights. Both wing loading and stall speed are calculated at 1g assuming steady level flight while using an estimation of C_{Lmax} created with AVL modeling and section lift data. Takeoff field length (TOFL) was computed via numerical integration in MATLAB using the drag polar, friction coefficients, and thrust available from the wind tunnel test data.

Load factor for each mission was calculated based on the wing-tip test requirement. A point load on the tip of the wing is equivalent to a 2.5g distributed load on the wing. Expected lift at this load factor was calculated based on estimated system weight, and then used to calculate load factor for Mission 1. In both cases, the value for load factor is intended to represent a maximum. Flight test data indicates that in-flight loads will be lower.

Mission 3 load factor was calculated with the expectation that the aircraft would not experience high loads. This arises because M3 does not require high speed flight, giving preservation of battery power a higher importance and allowing the mission to be flown as close to stall as possible. The relation between RPM and power consumption is more important than the increase in induced drag at high angles of attack. Low flight speed implies reduced lift over the wing so the load factor is reduced for a weight similar to M1.

The turn radius and time to complete a 360 degree turn were calculated for each mission using the mission's expected maximum velocity and allowable load factor.

The maximum velocity of the aircraft occurs at the point when the thrust required is equal to the thrust available. Thrust required is calculated using Equation 5.1 where $C_{D,0}$ and e are calculated in Section 4.4.3.



$$T_R = \frac{1}{2} \rho V^2 S C_{D,0} + \frac{2W}{\rho V^2 S \pi A Re} \quad (5.1)$$

Thrust available is taken from wind tunnel data gathered on the propulsion system chosen and is plotted in Figure 5.10 as discrete data points. A best-fit curve was calculated using Excel and extended to show the intersection of thrust available and thrust required.

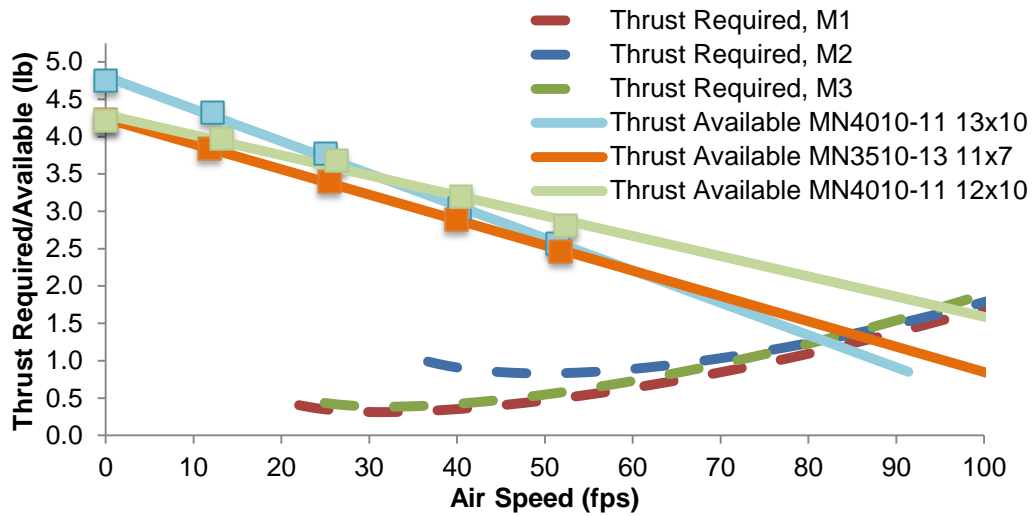


Figure 5.10: Thrust available and thrust required versus velocity. Solid lines are extrapolations of the wind tunnel data.

Figure 5.10 shows that the MN 3510-13 motor is inferior at all points along the expected flight regime. As a result, the motor selected was the MN 4010-11. Propeller selection was dependent on the specific mission. Since competition rules make it possible for teams to change the propeller used for each mission, the 12x10 propeller was chosen for M1 and M3. This combination has the highest thrust at speed, allowing for a higher maximum velocity. This is especially relevant for M1, where lap times are important. The 13x10 propeller was chosen for M2, as the 13x10 provides higher low end thrust, allowing for greater acceleration at low velocities and therefore reduced takeoff distance for the heaviest mission.

5.5.2 Mission Performance

The mission model described in Section 4.3 was used to estimate the final mission performance of the aircraft. The computed lap times represent an estimate that combines aerodynamics from AVL, power and current characteristics from wind tunnel data, and the physics of the mission model as described in Section 4.3. Figure 5.11 displays the projected first lap trajectories for Missions 1 and 2, with an initial ramp-up following takeoff and dips in velocity occurring at the turns. The remaining laps for Missions 1 and 2 are faster because they do not include takeoff. Table 5.5 shows the resulting estimated performance for each of the three missions with the selected propellers. The table also includes scoring estimates based on the updated analysis.

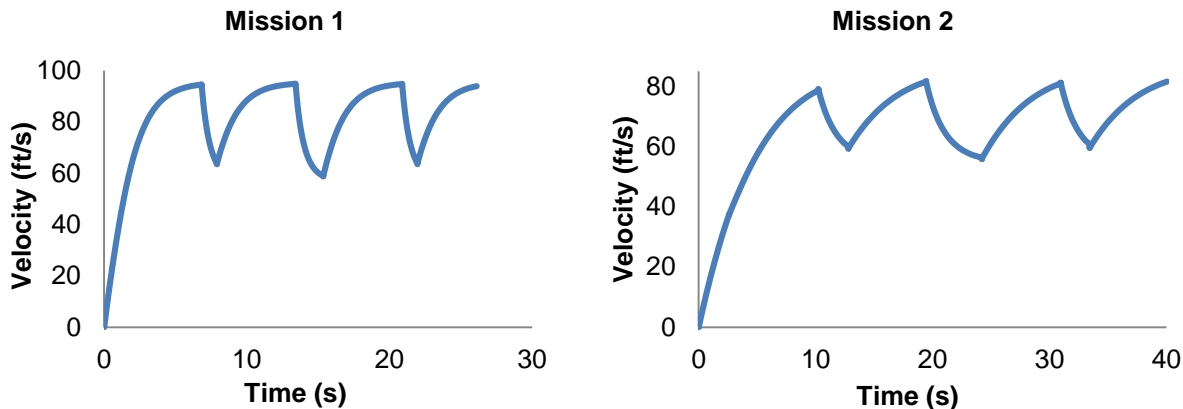


Figure 5.11: Simulation of Mission 1 and 2 lap trajectory.

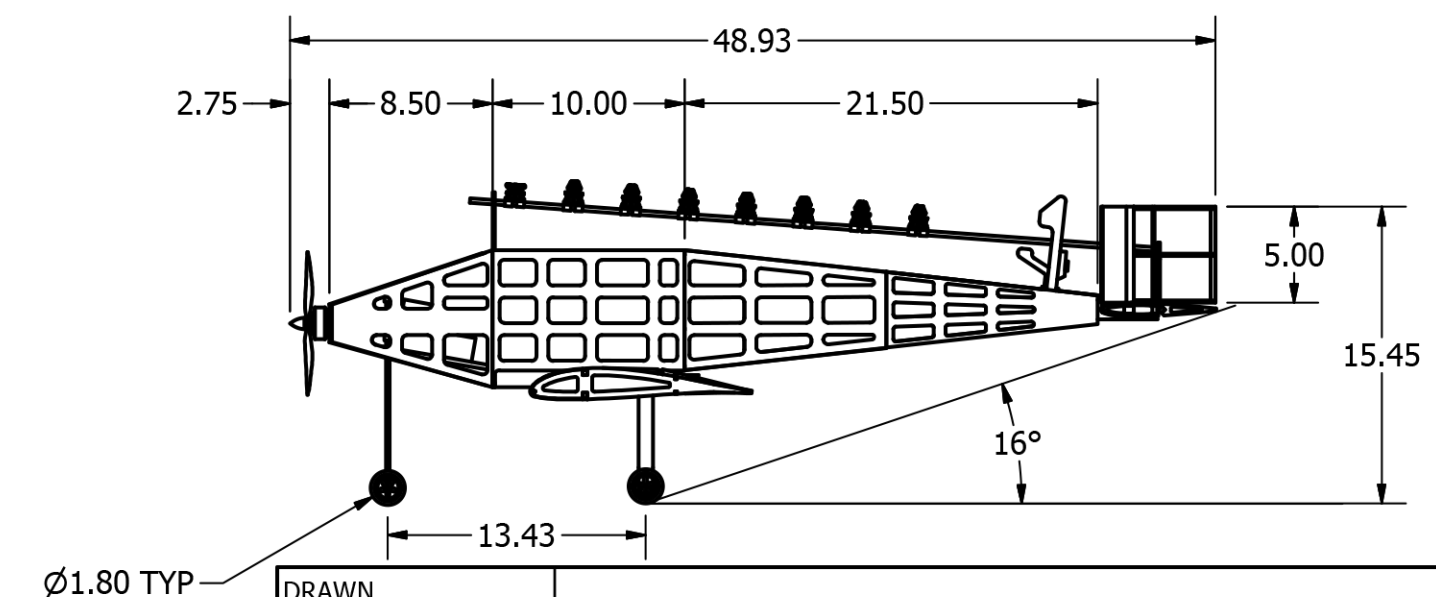
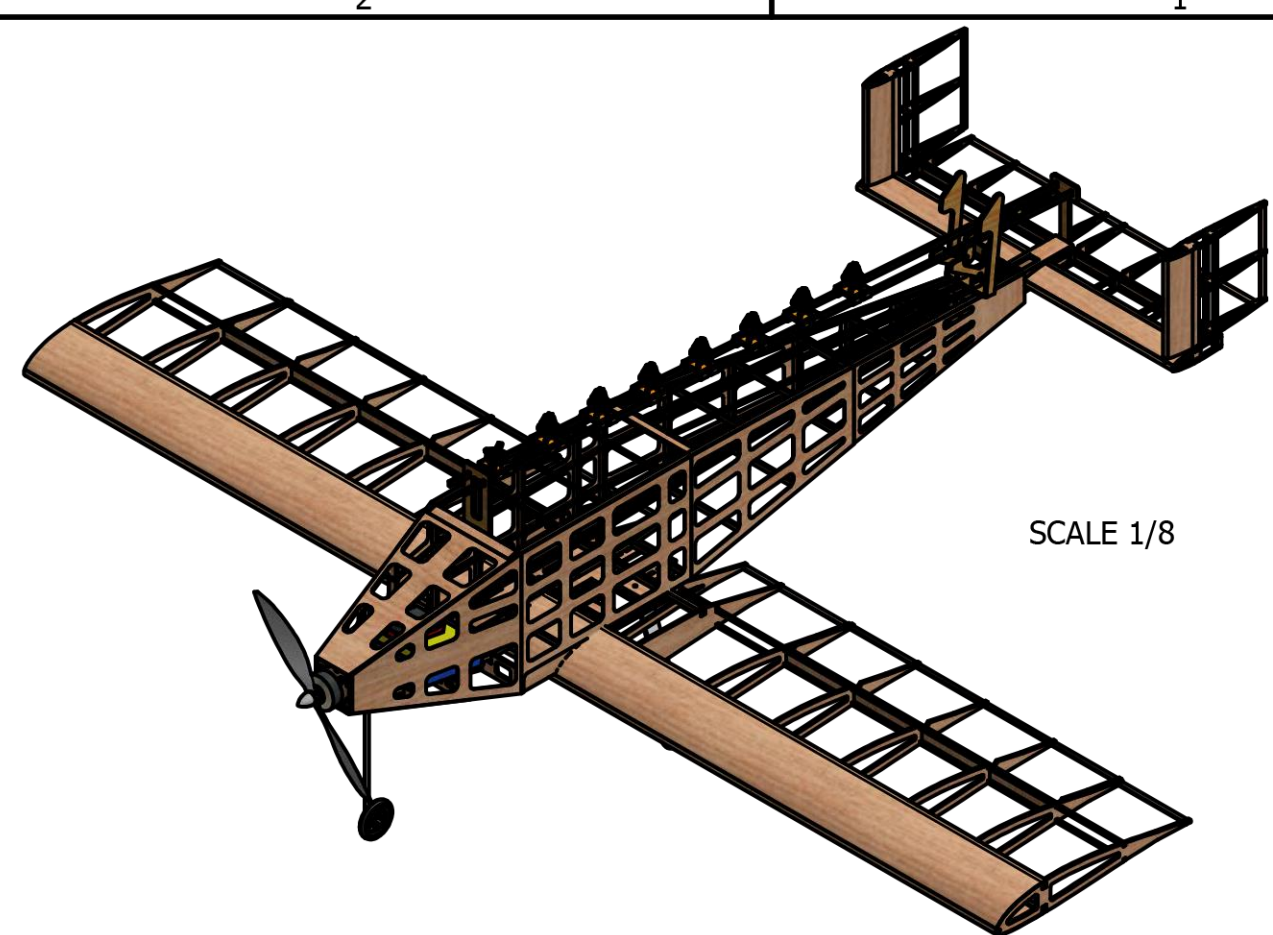
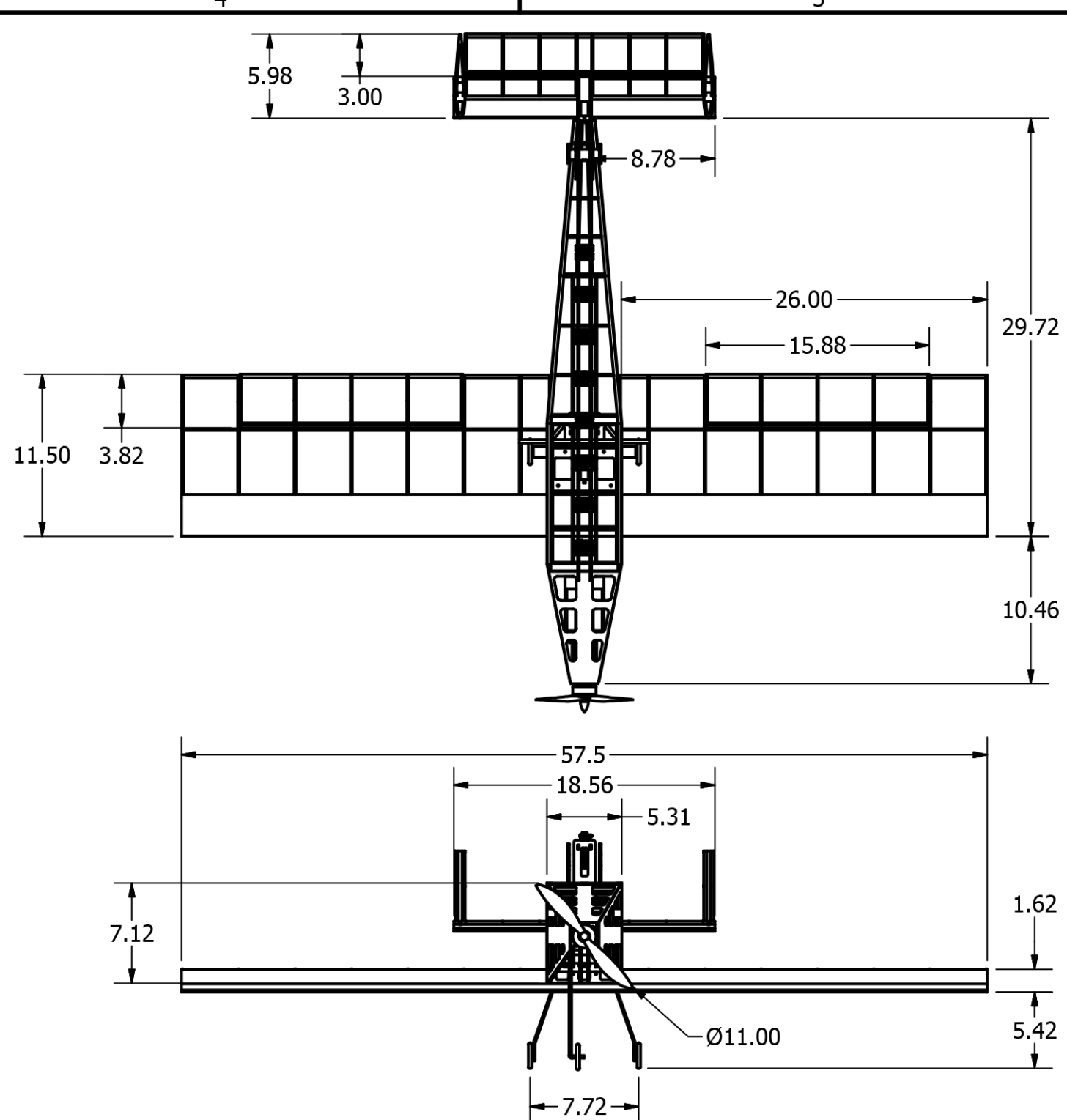
Table 5.5: Aircraft mission performance parameters.

Mission Parameter	Mission 1	Mission 2	Mission 3
W/S (psf)	0.653	1.742	0.828
Propeller Selection	12x10	13x10	12x10
Max Current (Amp)	19	19	19
Static Thrust (lbs)	2.30	2.30	2.30
1 st Lap Time (sec)	27.4	40.07	N/A
Mission Performance	8 laps in 4 minutes	120 seconds for 3 laps	8 balls
Mission Score	1.6	3.2	4.8
RAC	9.0	9.0	9.0

Based on the updated mission performance estimates shown in Table 5.5, the estimated FS is 9.6 while after normalization by RAC the score stands at 1.06.

5.6 Drawing Package

The following four pages illustrate the detailed CAD of *Buzz Killington*. The first sheet has the three-view diagram with relevant dimensions. The second sheet shows the structural arrangement of all major components. The third sheet displays the systems layout and location. The fourth sheet displays the payload arrangement for the internal and external payloads.

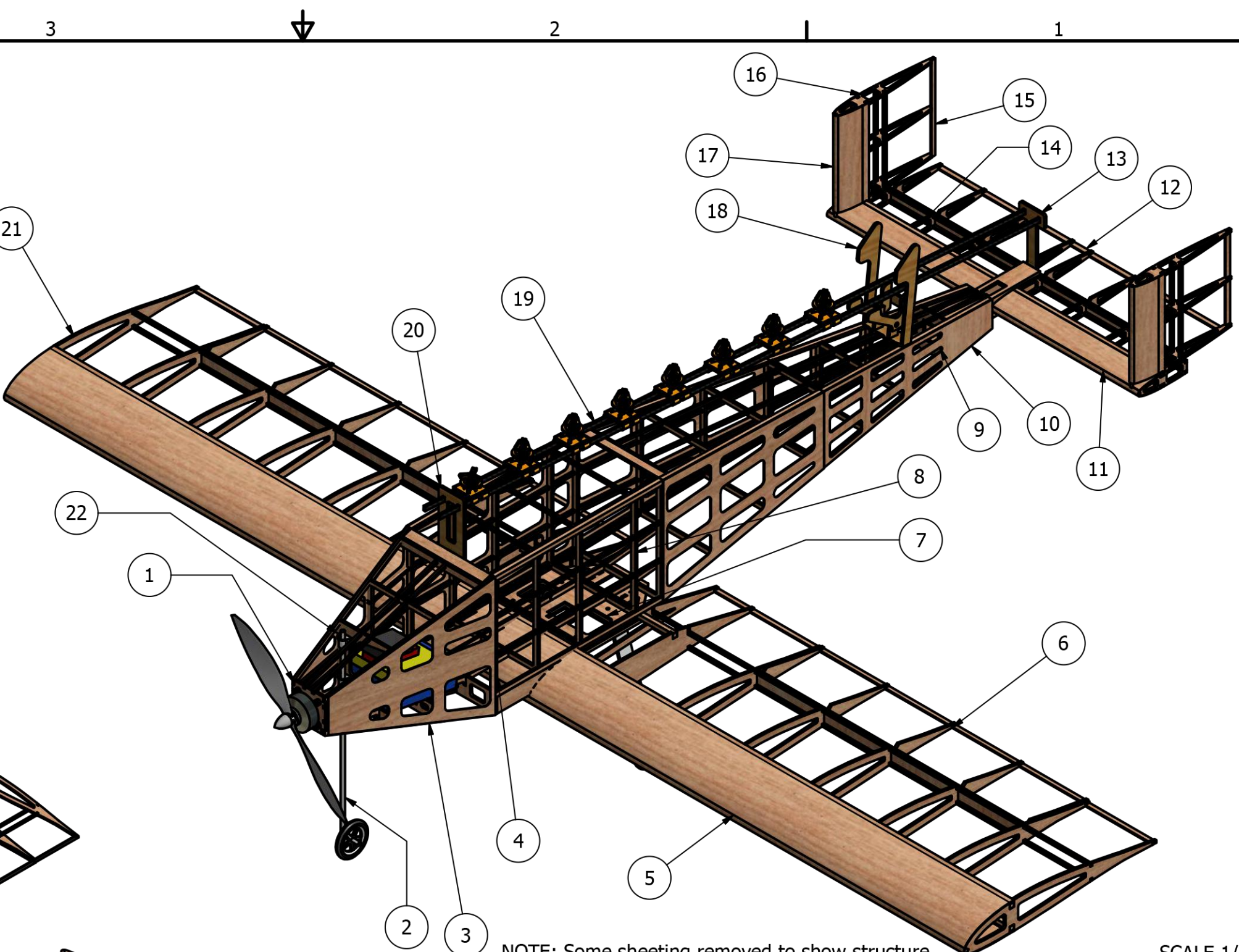
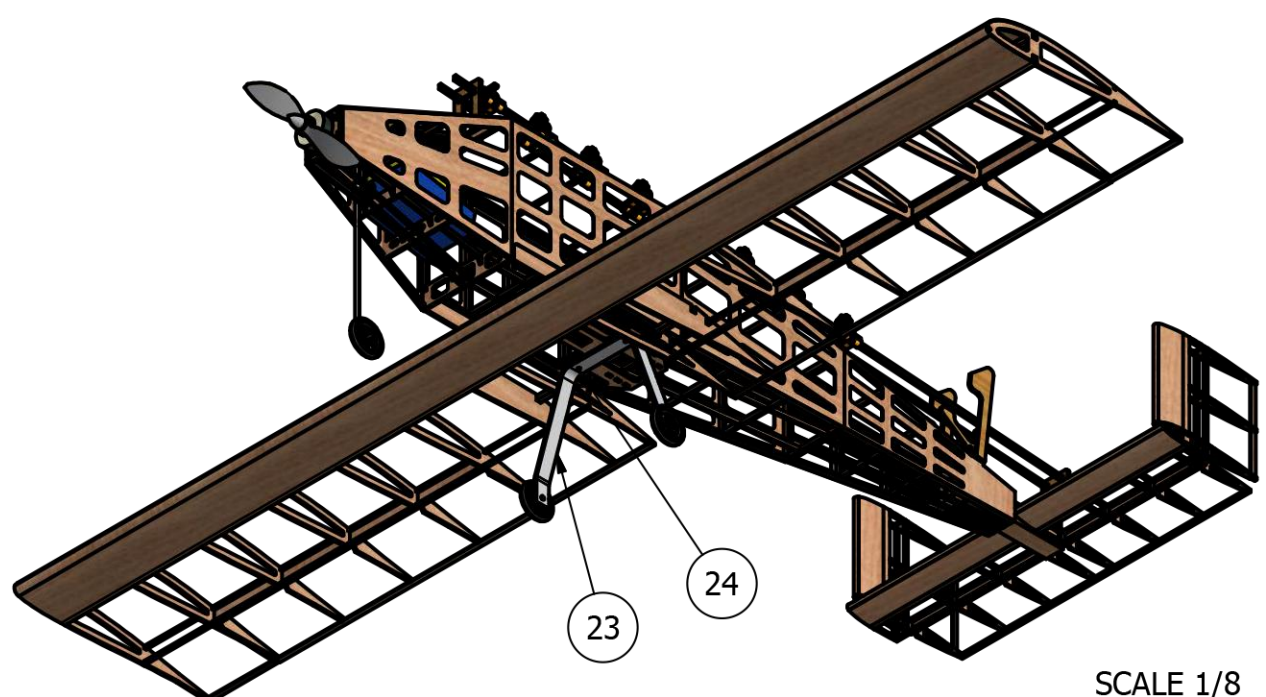


DRAWN
 David Gaitan
 CHECKED
 George P. Burdell
 2/19/2015

	SIZE B	DWG	
		Three View Drawing with Dimensions, M1 Configuration	
	SCALE 1/10	All Dimensions in Inches	SHEET 1 OF 4

Georgia Institute of Technology
 Buzz Killington

Parts List			
Item	Quantity	Part Name	Material
1	1	Motor Mount	Plywood
2	1	Nose Gear	Aluminum
3	9	Fuselage Sheeting	Balsa
4	12	Bulkhead	Balsa
5	2	Wing Sheeting	Balsa
6	2	Aileron	Balsa
7	1	Wing/Fuselage Joint	Plywood
8	2	Main Bulkhead	Plywood
9	1	Tail Attachment	Balsa
10	1	Empennage	Balsa
11	2	Horizontal Tail Sheeting	Balsa
12	1	Elevator	Balsa
13	1	Shuttle Retainer	Plywood
14	10	Horizontal Tail Ribs	Balsa
15	2	Vertical Tail	Balsa
16	6	Vertical Tail Ribs	Balsa
17	2	Vertical Tail Sheeting	Balsa
18	1	Ball Retainer	Plywood
19	2	Shuttle Rail	Carbon Fiber
20	1	Rail Holder	Plywood
21	16	Wing Rib	Balsa
22	2	Nose Gear Mount	ABS Plastic
23	1	Main Landing Gear Strut	Aluminum
24	2	Wing Attachment Bolts	No. 4 Steel Bolts



SCALE 1/8

4

3

2

4

1

2

SCALE 1/5

1

B

A

NOTE: Some sheeting removed to show structure

DRAWN David Gaitan	SIZE B	DWG Structural Arrangement Drawing
CHECKED George P. Burdell		
2/19/2015		
SCALE VARIES		SHEET 2 OF 4

Georgia Institute of Technology

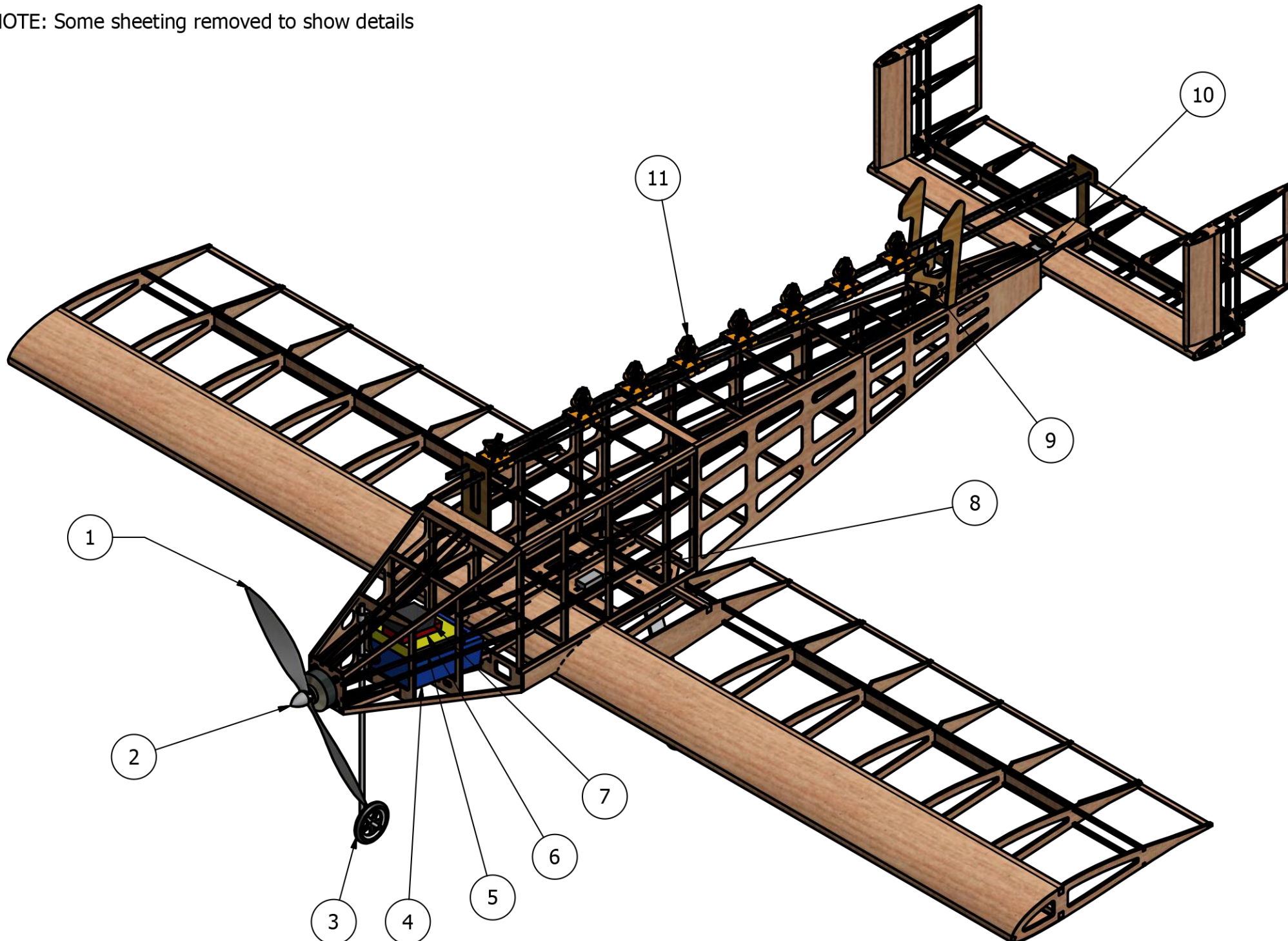
Buzz Killington

4
I3
I2
I1
I

Systems List

Item	Quantity	Item Name	Description
1	1	Propeller	APC 11 x 7
2	1	Motor	MN4010-11
3	3	Wheel	Rubber Tires
4	1	Main Battery	20 Cell NiMH, 1,500 mAh
5	1	Receiver Battery	4 Cell NiMH
6	1	Receiver	Futaba
7	1	Speed Controller	Phoenix 50
8	1	Aileron/Nose Gear Servo	BMS 380 Max
9	1	Ball Release Lever	Balsa
10	1	Elevator/Ball Release Servo	BMS 380 Max
11	8	Ball Shuttle	ABS Plastic

NOTE: Some sheeting removed to show details



DRAWN
David Gaitan
CHECKED
George P. Burdell
2/19/2015

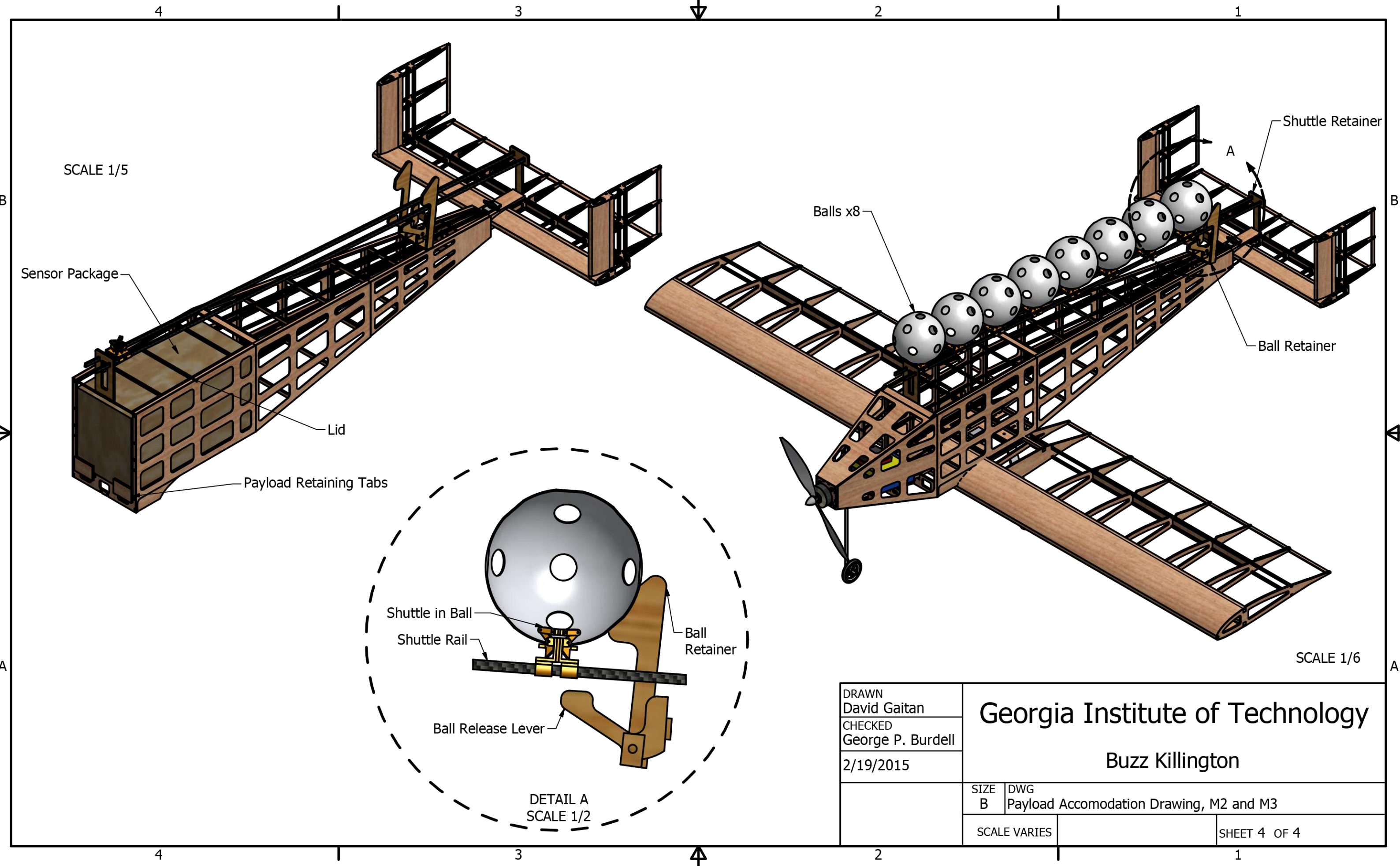
Georgia Institute of Technology

Buzz Killington

SIZE DWG
B Systems Layout Drawing

SCALE 1/5

SHEET 3 OF 4





6. MANUFACTURING PLAN AND PROCESSES

In order to design and build a competitive aircraft, the team considered various manufacturing processes and materials. The manufacturing process selected represented the best combination of weight, reparability, ease of manufacturing, team experience with the process, and cost.

6.1 Manufacturing Processes Investigated

The team had a wealth of experience using the well-established technique in built-up balsa wood manufacturing. However there were other viable manufacturing processes that could be superior. These processes were considered and qualitatively compared to the built up balsa technique using Figures of Merit, detailed below and summarized in Table 6.1.

Weight: similarly to conceptual design, weight is still the most important factor for any design decision, and is assigned a FOM of 5.

Reparability: With ever-present unknown factors, the reparability of the aircraft in case of an accident or a crash has to be accounted for, and was assigned a FOM of 2.

Ease of Manufacture: The ability to produce the aircraft to specification is critical to it performing according to predictions, and is directly related to Ease of Manufacture; it was therefore assigned a FOM of 3.

Experience: The team's knowledge was given some weighting because it relates to the ability of team members to produce quality results, as well as to refine existing techniques. However, since the team is always willing to learn new techniques, experience was only assigned a FOM of 2.

Cost: Keeping in mind that the team had limited resources, cost was inevitably added as a FOM. However, since the team emphasizes winning above all, cost was assigned a FOM of 1.

Table 6.1: Manufacturing FOM weighting.

Figure of Merit	0	1	2	3	4	5
Weight						5
Ease of Manufacture				3		
Reparability			2			
Experience			2			
Cost	1					

These Figures of Merit were used to investigate the manufacturing processes and materials common to remote control aircraft construction that were investigated detailed below.



Built-up Balsa: Stocks of competition grade balsa wood are laser cut from CAD models and glued together using cyanoacrylate (CA) adhesive to form the skeleton of the aircraft. It is then locally reinforced with more balsa or carbon fiber if necessary, and coated with Ultracote heat shrink film.

Foam Core Composite: Large blocks of foam are cut with a hot-wire or Computer Numerically Controlled (CNC) router to form the basic shape of the aircraft. Structural reinforcements are locally added if needed, and the entire foam-core is coated in fiberglass or carbon fiber, adding strength while providing an aerodynamic skin.

Molded Composite: This process is similar in principle to a foam core; however, the foam parts are only used to mold the composites and are then removed, with the fiberglass or carbon fiber acting as the primary structure.

The processes were evaluated against each other by assigning each one a FOM score, with a score of five indicating a superior choice, three an average choice, and one equaling an inferior choice. All methods were assumed to result in an aircraft designed for an identical load. The results of the comparison are summarized in Table 6.2.

Table 6.2: Weighting for various manufacturing techniques.

		Manufacturing Process		
FOM	Value	Built-up Balsa	Foam Core Composites	Molded Composites
Weight	5	5	3	5
Ease of Manufacture	3	3	3	1
Reparability	2	3	1	1
Experience	2	5	3	3
Cost	1	5	3	1
Total	13	55	35	37

Based on the Figures of Merit, built-up balsa was considered the best method for the plane manufacturing. To further confirm this choice, the team laid-up a molded composite wing section, the second-best candidate of the assessment above. The section consisted of 3 oz/yd² fiberglass with 1/32" balsa core, and resulted in an area density of 0.12 lbs per square foot of skin. With nearly 10 ft² of wetted area, the wing alone would weigh 1.2 lbs, more than the entire balsawood structure of the aircraft as-built. Therefore, the built-up balsa technique was used to construct the aircraft.

6.2 Manufacturing Processes Selected

The team used the above comparison to optimize the built-up balsa technique to achieve the most competitive aircraft by having the lightest structure possible in accordance with competition rules without sacrificing structural integrity. This optimized technique is detailed in Table 6.3:



Table 6.3: Built-up balsa manufacturing technique.

Manufacturing Component	Material / Technique
Principal material	Competition Grade balsa wood
Other materials	Local fiber reinforcements
Adhesive	CA, or epoxy if needed
Coating	Ultracote
Part manufacture	CAD-guided laser cutting
Part assembly	Designed-to-fit jigsaw pieces

Of the many different ways to apply built-up balsa, the team chose specific techniques and materials that would minimize the aircraft structure's weight without compromising its strength. These strategies are:

Selective Material Use: Since balsa wood can vary significantly in density and strength, the team sorted its entire stock of balsa by weight. The lightest pieces were selected for construction and were sent to the team's laser cutter, with the lightest of the cut parts reserved for the final competition aircraft.

Local Reinforcements: Due to the very low density of balsa used, the aircraft structure lacked strength in several key locations. Rather than compensate by over-building the entire aircraft, these locations were reinforced with composite or additional balsa, increasing strength with minimal penalty in weight.

Selective Shear Webbing: The wing for this aircraft provided an uncommon structural challenge for the team due to the requirement of containing the minimum amount of servos. The need for the servo that controls the ailerons of the wing to also control the nose gear introduced a large amount of torque on the wing. The team employs shear webbing in the bays adjacent to the servo attachment points to provide additional stiffness. The wing structure can be seen in Figure 6.1.



Figure 6.1: Prototype aircraft wing in production.



Lightening Holes: The use of a concentrated and localized structure caused most structural members to not experience significant loading. Where possible, the team laser-cut lightening holes into ribs and bulkheads to reduce weight with little losses in the overall stiffness and strength of the aircraft.

3-D Printing: Traditionally, parts are laser cut from balsa wood or milled from aluminum. However, the integration of additive manufacturing techniques allowed for the creation of light, custom, components that maintain torsional stiffness and resistance to shear stress. Additive manufacturing is becoming a more important part of aerospace manufacturing; the use of these techniques also provides valuable experience for team members. 3-D printing was used to create a reliable drop mechanism.

Coating: Most balsa aircraft are coated with a heat shrink adhesive infused plastic covering material called Monokote, which is durable and easy to handle. However, the team chose to use a more delicate plastic covering, Ultracote, because it is significantly lighter.

6.3 Manufacturing Milestones

A milestone chart was established at the beginning of aircraft manufacturing to ensure a logical, consistent order was followed during construction. Progress was recorded and monitored by the team leader to ensure all major milestones were met. The milestone chart is shown below in Figure 6.2, capturing the planned and actual timing of major events.

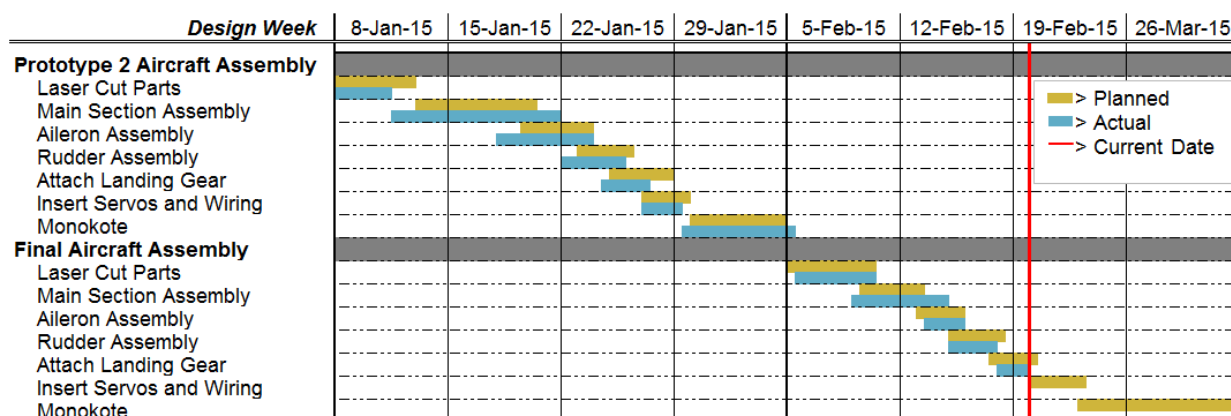


Figure 6.2: Aircraft manufacturing milestone chart showing planned and actual timing of objectives.

7. TESTING PLAN

A plan for an extensive testing campaign to validate the aircraft, and its components, was created to determine what configurations and subsystems would be the most capable. Testing culminates in test flying a full round of competition flights on the final competition airframe.



7.1 Objectives and Schedules

The testing was broken up into three main categories: propulsion, structures, and performance. The propulsion and structures subsystems were tested before flying the whole aircraft to gain knowledge and set realistic and useful objectives at each test flight. A breakdown of the testing schedule is displayed in the following Gantt chart, shown in Figure 7.1:

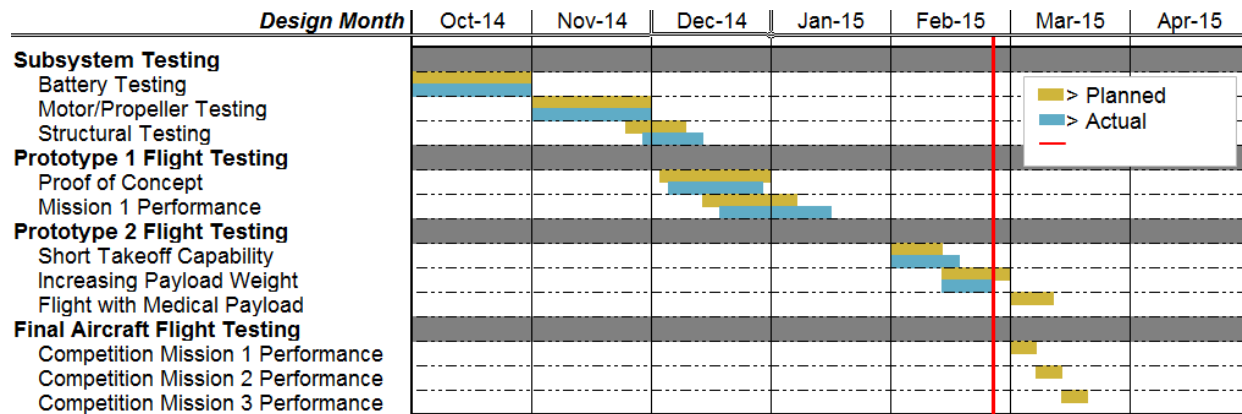


Figure 7.1: Aircraft and subsystem testing milestone chart showing planned and actual timing of objectives.

7.2 Propulsion Testing

The objectives for the propulsion testing were to determine which of the two motors would be best for the flight missions. The motors and propellers tested were based on MotoCalc predictions as expressed in Section 4.2. Thrust versus velocity for vehicle performance and power draw for motor performance for each motor propeller combination were determined using measurements of thrust, torque, RPM, voltage, and current draw. Using data obtained from testing, the team was able to compare the actual performance of the motors to the MotoCalc predictions in order to gather a better estimate of actual performance. This information allowed the team to select the best propulsion system to achieve the best score possible.

A rig that included load cells to calculate thrust and torque as well as an electric motor measurement system was constructed for the wind tunnel testing, and is shown in Figure 7.2. The electric motor parameters were monitored with an EagleTree system that records the RPM, voltage, and current draw of the motor. Custom written software was used to collect the torque and thrust values as well as to remotely control the motor for 30-second intervals with 10-second full thrust intervals and 10-second acceleration and deceleration intervals.

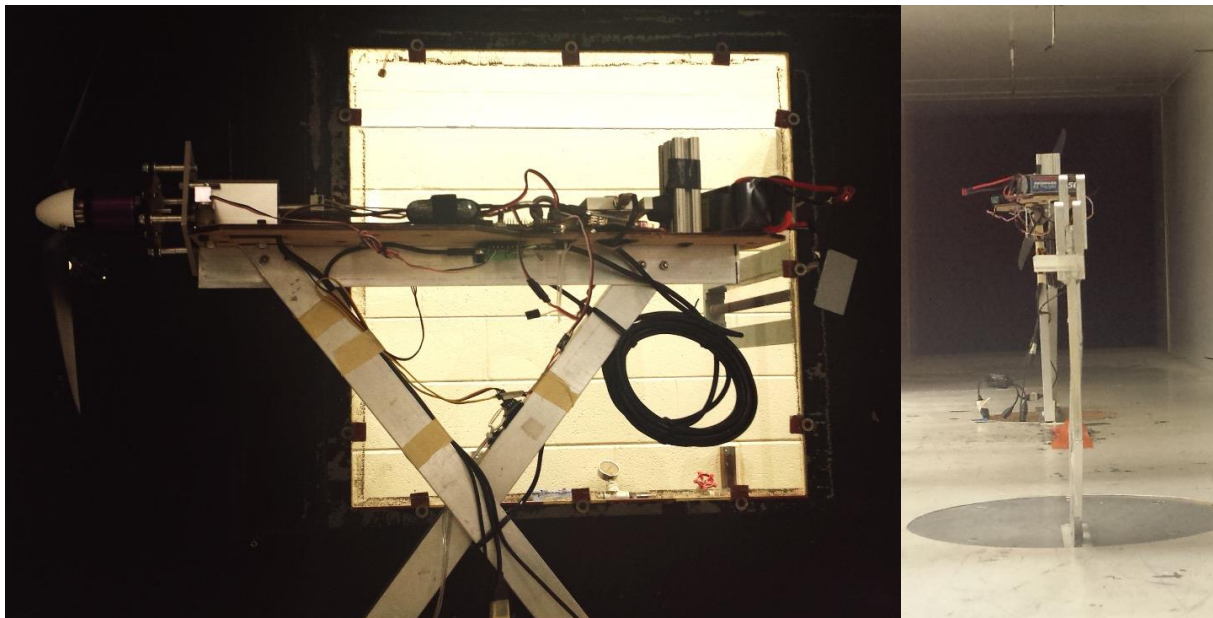


Figure 7.2: Picture of thrust test rig in wind tunnel.

The team utilized the Georgia Tech Low Turbulence Wind Tunnel to conduct its wind tunnel tests. The wind tunnel is powered by a fan which forces air through a series of honeycombed grates creating a smooth, even flow of air. The fan creates airflow with a maximum airspeed of about 52 feet per second. The wind tunnel creates an environment closely resembling actual flight conditions and thus providing accurate motor and propeller efficiencies. By testing different combinations of motors and propellers, these efficiencies were contrasted to find the best combinations for each mission. The results are described in Section 8.1.

7.3 Payload Loading and Release Testing

An experimental trade study was performed to determine the relationship between the amount of payload and total loading time. The GS was simulated using a team of three individuals. One team member would hold the aircraft while the other two loaded the payload. Since the distance from the safe zone to the loading area was not specified, the team did all test runs starting 20 ft. from the loading zone. This distance was chosen due to it being the distance to the loading zone at the 2013-2014 AIAA DBF competition GS. The team conducted a timed loading sequence in which the M2 payload was installed into the aircraft. The team then conducted a second timed sequence in which it unloaded the M2 payload and installed the M3 payload. Using the times found in this study it was determined the greatest time cost in the GS was due to the number of balls used in M3.

The most important aspect of the drop mechanism is its reliability. The goal of M3 is to drop a single ball for each lap flown, and if multiple balls are dropped in the drop zone during one lap, the lap is invalidated.



Therefore extensive testing was conducted in order to validate the reliability of the drop mechanism. The drop testing mechanisms was initially tested in a controlled static case for proof of concept. The team utilized the Georgia Tech Low Speed Wind Tunnel in order to test how the drop rig acted in air flow at different angles of attack and sideslip, to determine all possible orientations the drop mechanism could perform at. Finally the aircraft was flight tested with the drop mechanisms to validate the reliability in true flight.

7.4 Structural Testing

To validate the design of the wings, the aircraft was subjected to a wing tip test. A wing tip test simulates the maximum loading the wings would experience in flight by loading the payload bay with the maximum weight and lifting the plane by the wing tip. The tip test simulates a maneuver resulting in a root bending moment of 2.5g.

7.5 Flight Testing

Flight testing was conducted across two airframes. Each airframe represents an iteration of the design. The first airframe, the initial prototype, was used to determine the flying qualities of the aircraft design. Verification of structural layout and load estimates were also conducted. Initial testing of a simulated M1 profile was flown.

The second airframe is currently being used as a testing platform. Changes were made to the design based on pilot feedback about Airframe One. These included modifications to the fuselage and vertical tail to improve handling qualities and optimization of M2 and M3 payload integration. After initial evaluation of flight qualities, both M2 and M3 were simulated.

Evaluation of M2 and M3 mission performance of Airframe Two is ongoing. Experience and data gained from Airframe Two will be used to improve the design for Airframe Three, which is intended to be the final competition aircraft. Airframe Three will then fly simulations of all three flight missions to determine the performance. The schedule and flight order is displayed in Table 7.1, seen below.



Table 7.1: Flight test goals and order.

Flight Test	Aircraft	Goal
1	Prototype	Maiden flight, determine flying qualities
2	Prototype	Takeoff distance, stall and recovery tests
3	Prototype	Mission 1 simulation
4	Prototype 2	Determine flying qualities, takeoff distance tests
5	Prototype 2	First flight with payload
6	Prototype 2	Maximum payload test
7	Prototype 2	Ball payload test
8	Final	Mission 1 performance
9	Final	Mission 2 performance
10	Final	Mission 3 performance

7.6 Checklists

Various tests have specific procedures which must be followed accurately to produce the desired objectives and ensure safety. This section lists the checklists utilized by *Buzz Killington* while conducting tests that required a significant amount of steps, such as propulsion and flight testing.

7.6.1 Propulsion Test Checklist

The checklist in Table 7.2 was created to ensure safety while dealing with propellers and electrical equipment, and to make sure the test is not wasted due to some mistake in preparation. This checklist was used in the testing of all motor, battery and propeller combinations.

Table 7.2: Propulsion testing checklist.

Propulsion Test Checklist					
1. Propeller secured?	<input type="checkbox"/>	2. Motor mount secured?	<input type="checkbox"/>	3. All plugs secured?	<input type="checkbox"/>
4. Batteries peaked?	<input type="checkbox"/>	5. Throttle down?	<input type="checkbox"/>	6. Data system on?	<input type="checkbox"/>
7. Custom code running?	<input type="checkbox"/>	8. All clear of testing rig?	<input type="checkbox"/>	9. Wind tunnel closed?	<input type="checkbox"/>

7.6.2 Flight Test Checklist

The checklist in Table 7.3 was created with the important goal of preventing any system from malfunctioning in mid-air, which could lead to the aircraft crashing; its thorough execution is paramount to the team's success, and it will be used at the DBF event as well.



Table 7.3: Pre-flight checklist.

General System Checks									
Structural Integrity		Center of Gravity Location		Time	Date				
		X:		Y:					
Payload									
Internal									
Primary Bay			Propulsion Bay						
Laterally Secure?		Hatch Secure?		Battery Pack	Receiver Pack	Secure?			
External									
Attachment secure?		Pins locked?		Clear of Jams?					
Control Surfaces									
Ailerons			Elevator						
Deflects?	Glued?	Slop?	Deflects?	Glued?	Slop?				
Electronics and Propulsion									
Receiver Battery Charged?	Primary Battery Charged?	Receiver/Transmitter Go?	Wires secure?	Battery hot?	Prop secure?	Prop direction?			
Weather									
Wind speed		Wind Direction		Temperature					
Initials for Approval									
Chief Engineer		Pilot		Advisor					

8. Performance Results

8.1 Component and Subsystem Performance

8.1.1 Propulsion

Batteries: A 10-cell, 1500mAh NiMH battery pack was discharged at 5 amps (3.3 times its capacity) and at 15 amps (10 times its capacity) to characterize the discharge capabilities of the NiMH batteries. The resulting data is shown in Figure 8.1 on a per cell basis. NiMH battery cells have a nominal voltage of 1.2V, and the 5 amp discharge curve is capable of maintaining this voltage. However, at the higher discharge rate of 15 amps the cell voltage continuously drops. The result of this is a small decrease in the effective power that can be drawn from the batteries. However, the higher current draw of the 15 amp discharge is necessary for the propulsion system to generate the power required for the aircraft.

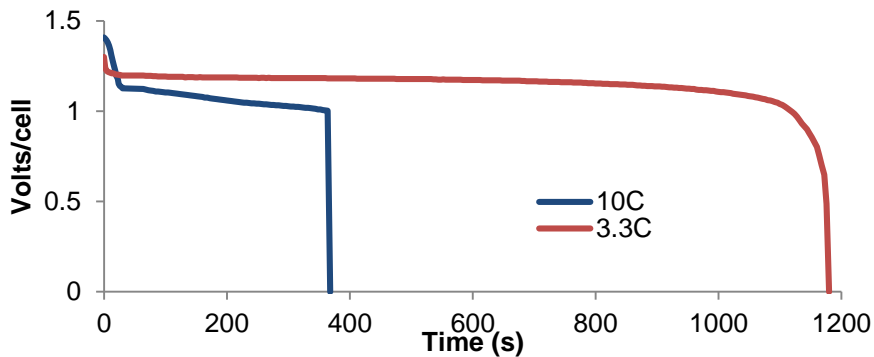


Figure 8.1: Battery discharge rates.

Motors and Propellers: Three motor-prop combinations were tested, based on the calculations described in Section 4. These combinations were modeled within MotoCalc, then the results verified against wind tunnel data. Figure 8.2 gives the efficiency curves for all three motor-prop combinations. Figure 8.3 gives the thrust curves for all three motor-prop combinations.

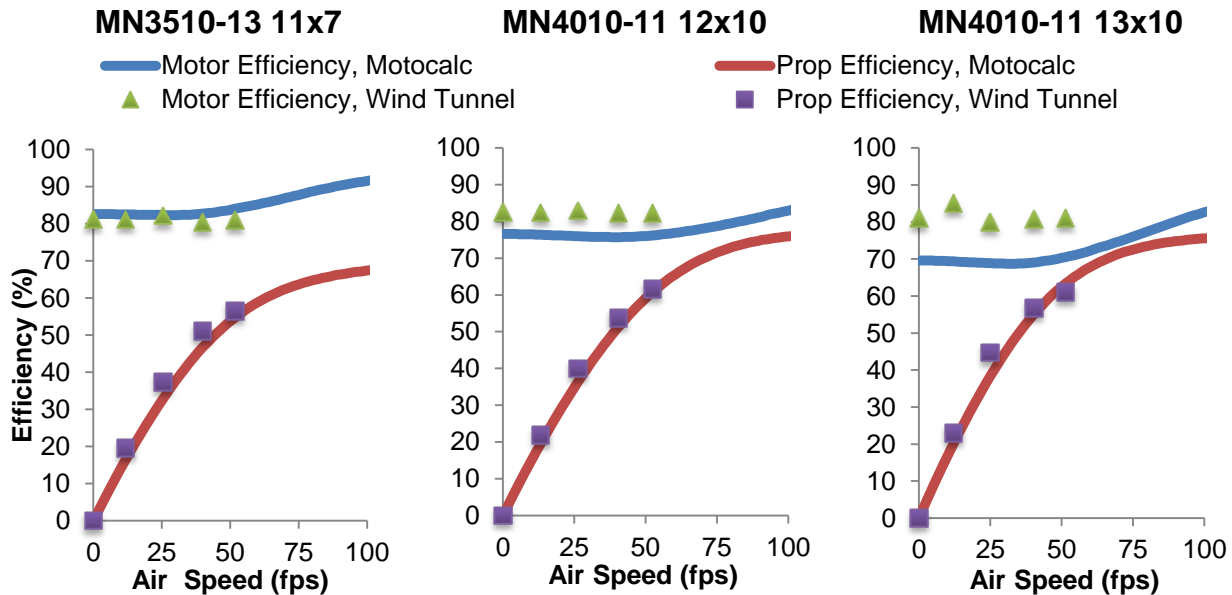


Figure 8.2: Motor efficiencies predicted by MotoCalc and wind tunnel testing.

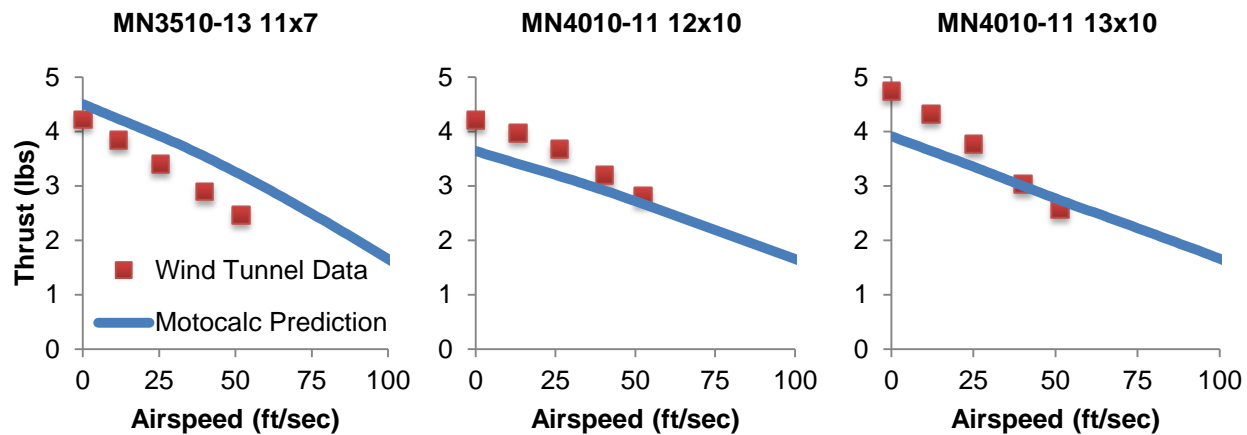


Figure 8.3: Error between motor efficiencies predicted by MotoCalc and wind tunnel testing.

Figure 8.2 shows that the motor and propeller efficiencies predicted by MotoCalc are largely corroborated by the wind tunnel data. Figure 8.3, however, demonstrates significant discrepancies in the thrust prediction. MotoCalc over predicts the thrust for the Tiger MN 3510-13, but under predicts thrust for the MN 4010-11. This drove the selection of the latter as the final propulsion system. The difference between the two data sources potentially arises from the propeller model used in MotoCalc. While the efficiency curves are well aligned, it is possible that MotoCalc's propeller calculation method causes the error in thrust. Further investigation is necessary to determine the exact cause of the discrepancy, and to evaluate alternative propulsion analysis methods.

8.1.2 Structural Tests

Wing Testing Results: The full size airplane was subjected to the required wing tip testing specified in the rules as part of the technical inspection process. This was done by loading the full internal Mission 2 payload of three blocks into the payload bay, then lifting the airplane by the wing tips. The successful wing tip test is shown in Figure 8.4.

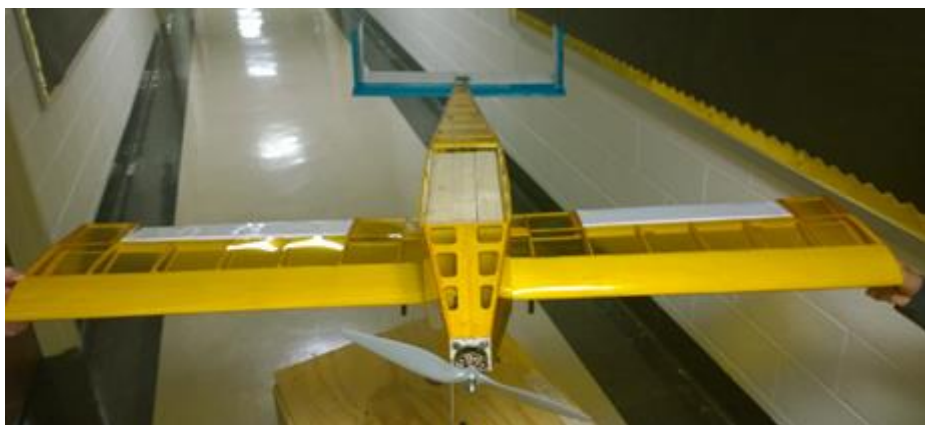


Figure 8.4: Wingtip Structural Test with Full Payload.



8.2 System Performance

A loading time test determined the time required to run from the safe zone to the aircraft and load the M2 payload was 12 seconds. This time was assumed to be constant for each run. The M3 loading time was then timed using the method described in Section 7.3. Initially the time required to load a single ball was 2.0 seconds. The team believes the time to load a single ball can be decreased to the predicted time of 1.5 through practice. Summing the floor M2 payload time of 12 seconds with the fastest ball loading time of 2.0 seconds per ball, it was found that the team could achieve a total loading time of 28 seconds with a minimum possible time of 24 seconds. A picture taken during a loading test is shown in Figure 8.5.



Figure 8.5: Payload Loading Time Testing.

Flight tests of *Buzz Killington* were performed to evaluate the performance of the aircraft and validate the performance predictions. The results indicate the performance predictions were realistic. Further optimization and increasing pilot familiarity with the system should improve system performance to meet or exceed the predicted performance.

To evaluate system performance during flight testing beyond simple lap timing and takeoff performance, the team equipped the aircraft with a data collection system that could be used to compare to the estimated mission performance in Section 5. The team purpose-built an Arduino-based telemetry system with a live data feed. On a number of test flights, the Arduino was mounted to the aircraft and recorded



GPS at 1 Hz to yield trajectory data. An example of a full lap trajectory is displayed in Figure 8.6 superimposed on satellite imagery using Google Earth.



Figure 8.6: Trajectory of aircraft during competition laps from GPS data.

The results of flight testing are shown in Table 8.1:

Table 8.1: Comparison of Predicted and Actual Performance Averages.

	1 st Lap Time (s)		Time for 360		Balls Carried		TOFL	
	Predicted	Actual	Predicted	Actual	Predicted	Actual	Predicted	Actual
M1	27.4	33.1	3.49	3.15	-	-	6.72	17
M2	40.07	54.2	7.45	8.46	-	-	53.2	57
M3	-	-	-	-	8	2	10.76	15

Discrepancies between predicted and actual times for a 360 degree turn are low. Much of the difference between the two figures can be explained by pilot behavior. In all cases, time for a 360 degree turn was predicted assuming maximum velocity. However, during testing, the pilot tended to reduce speed slightly when going into a turn, which reduced the turn radius. For M3, the discrepancy was due to the test pilot flying conservatively so as not to inadvertently over stress the aircraft in a turn. These discrepancies could be caused by inconsistent turning radii of the pilot compared to an ideal turn.

Discrepancies between predicted and actual TOFL vary significantly for M1 and M3, and slightly for M2. While M2 takeoff distance is currently within competition bounds, a reduction in weight to increase the safety margin is necessary. M1 and M3 discrepancies are a result of differences between pilot actual behavior and assumed behavior. The model used for calculating TOFL assumes that the pilot immediately advances to maximum throttle, but the pilot has been taking off more conservatively to maintain ground steering.



Buzz Killington can achieve a total of 7 laps in four minutes for M1 based on the recorded flight times. Further optimization of the system is required to achieve 8 laps. The team plans to accomplish this by decreasing the landing gear height to reduce weight and drag. In addition, increasing pilot familiarity with the system will allow for a reduction in lap times. The team believes with these optimizations, 8 laps can be achieved as predicted.

Flight testing was also used to validate M3 feasibility. Testing has not completed full M3 laps at this time, but it is expected that the aircraft will be able to complete all laps required for M3 without exhausting the batteries. Testing demonstrates that the drop mechanism described within Section 5.3.5 is fully capable of dropping one ball, on command, without requiring an unsafe acrobatic maneuver. The aircraft is shown dropping a ball during a test flight in Figure 8.7.

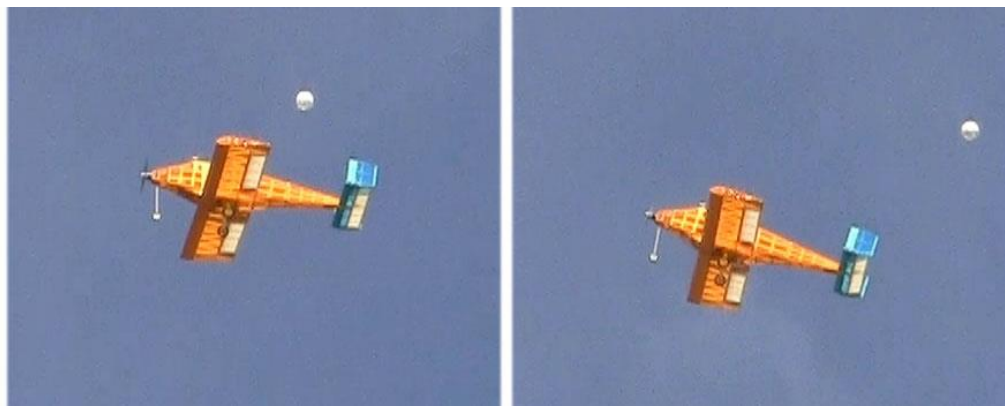


Figure 8.7: In flight release of payload.

In summary, as of the time of this report, seventeen flight tests have been performed on two different prototypes. Although flight testing revealed Mission 1 scores may be lower at the competition than analysis predicted, the research, component selection, and testing that fed into the design process resulted in a lightweight aircraft capable of lifting three blocks for Mission 2, drop payload successfully for Mission 3, all without suffering major losses to speed. The concept of a single-engine, low wing, conventional aircraft proved to be successful in completing the loading mission and all flight missions, and was proven through laboratory testing to be lighter than other designs of an equivalent power level. The *Buzz Killington* team is eagerly awaiting more testing opportunities to ensure success during all missions at the competition and hone pilot familiarity with the aircraft. The team is confident that the overall configuration for *Buzz Killington* as shown in Figure 8.8 has the best scoring potential, and is positioned to place well in Tucson.



Figure 8.8: Final Aircraft.

9. REFERENCES

- Anderson. J. D. *Fundamentals of Aerodynamics*, 4th edition, McGraw Hill.
- Bauchau, O. A., & Craig, J. I. (January 7, 2009). *Aerospace Structural Analysis*. Springer.
- Drela, M., & Youngren, H. (2008, 08 04). *AVL*. Retrieved 01 10, 2009, from [http://web.mit.edu/drela/Public/web/avl/].
- Drela, M., & Youngren, H. (2008, 04 07). *XFOIL*. Retrieved 10 01 2008, from Subsonic Airfoil Development System: [http://web.mit.edu/drela/Public/web/xfoil/].
- Hoerner, Sighard F. *Fluid Dynamic Drag*. 2nd. Published by author, 1965.
- Katz, Joseph and Maskew, Brian. "Unsteady low-speed aerodynamic model for complete aircraft configurations," *Journal of Aircraft*. Vol. 25, pp. 302-310. Apr. 1988.
- McDaniel, Katie et al. (2008). *Georgia Institute of Technology Team Buzzed*. Editor: Johnson, Carl.
- Phillips, Warren F. *Mechanics of Flight*. 1st. Hoboken, NJ: Wiley, 2004.
- Roskam, Jan. *Airplane Design Part VI*. Darcorp, 2000.
- Roskam, Jan. *Airplane Flight Dynamics and Automatic Flight Controls Part I*. Darcorp, 2007.
- Selig, M. (2008, 02 19). *UIUC Airfoil Data Site*. Retrieved 10 01, 2008, from [www.ae.uiuc.edu/m-selig/ads.html].